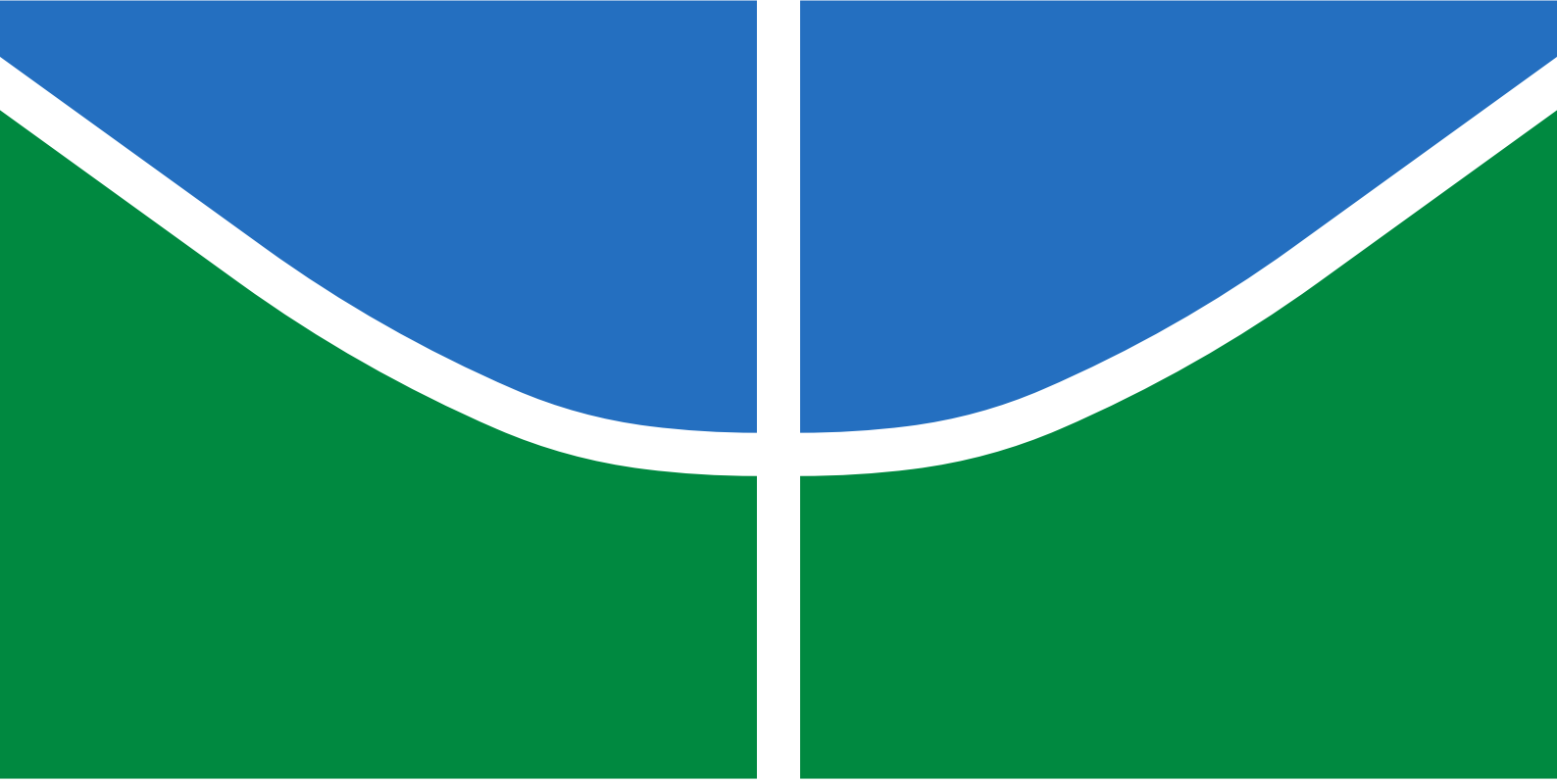

TRABALHO DE GRADUAÇÃO

Cooperative MIMO for Wireless Sensor Network and Antenna Array based Solutions for Unmanned Aerial Vehicles

Marco Antonio Marques Marinho

Brasília, janeiro de 2013

UNIVERSIDADE DE BRASÍLIA

FACULDADE DE TECNOLOGIA

UNIVERSIDADE DE BRASILIA
Faculdade de Tecnologia

TRABALHO DE GRADUAÇÃO

Cooperative MIMO for Wireless Sensor Network and Antenna Array based Solutions for Unmanned Aerial Vehicles

Marco Antonio Marques Marinho

Relatório submetido ao Departamento de Engenharia Elétrica como requisito parcial para obtenção do grau de Engenheiro de Redes de Comunicação

Banca Examinadora

Prof. Dr.-Ing. João Paulo Carvalho Lustosa da Costa
Orientador _____

Prof. Dr. Edison Pignaton de Freitas
Coorientador _____

Prof. Dr. Rafael Timóteo de Sousa Júnior
Examinador interno _____

Prof. Dr. Ricardo Zelenovsky
Examinador interno _____

Dedicatória

Aos meus pais:
Marco Antonio e Marcelita, amores maiores da minha vida. Não se pode pedir por pais melhores.

Ao meu irmão:
Murilo, eterno amigo, companheiro e fonte de inspiração.

Aos meus avós:
Pedro e Juvercina (in memoriam), sinto sua falta.

Marco Antonio Marques Marinho

Agradecimentos

Em especial, aos meus professores e orientadores, João Paulo Carvalho Lustosa da Costa e Edison Pignaton de Freitas, responsáveis por reacender meu interesse pela vida acadêmica e a quem serei eternamente grato por minha formação científica, pela paciência, incentivo, amizade e excelente orientação ao longo de inúmeros trabalhos. Por sua generosa colaboração, quaisquer agradecimentos seriam insuficientes para exprimir todo o meu respeito, gratidão e admiração.

Ao meu amigo e colega de curso, Ronaldo, pelas inúmeras discussões, debates e sugestões, tanto em temas acadêmicos quanto fora deles.

À Clarissa, que tanto sofreu com minha ausência quando da elaboração desta monografia e dos diversos trabalhos ao longo dos últimos anos, pela paciência, carinho e companhia e amor inestimáveis e por tornar minha vida uma experiência maravilhosa.

Marco Antonio Marques Marinho

RESUMO

A crescente miniaturização e barateamento dos componentes eletrônicos viabilizou a utilização de redes de sensores sem fio para os mais diversos fins, desde a prevenção de catástrofes a monitoração de pacientes em hospitais. Esses dispositivos são geralmente movidos a bateria e apresentam grande restrição em suas dimensões físicas o que torna imperativo que sua eficiência energética seja maximizada. A aplicação de veículos aéreos não tripulados (VANTs) em conjunto com redes de sensores tem se apresentado como uma solução viável para a manutenção da comunicação entre os nós da rede. Técnicas que utilizam múltiplas antenas podem ser aplicadas para minimizar o consumo de energia em redes de sensores e auxiliar na comunicação destas redes com grupos de VANTs. O mesmo conjunto de antenas utilizado nos VANTs para a comunicação pode ser aproveitado para prover outros benefícios, como a implementação de um altímetro preciso e de um sistema de posicionamento que não depende de agentes externos. Este trabalho apresenta um conjunto de técnicas de arranjos de antenas capaz de melhorar a eficiência de redes de sensores, proporcionar controle automatizado e seguro para VANTs e possibilitar uma interação eficiente entre esses dois sistemas.

Palavras Chave: Veículo Aéreo Não Tripulado, Redes de Sensores, MIMO, Conjunto de Antennas

ABSTRACT

The cheapening and increasing miniaturization of electronic components has enabled the use of wireless sensor networks for various purposes, from disaster prevention to patient monitoring in hospitals. These devices are generally battery powered and have great restrictions in its physical dimensions which makes it imperative that their energy efficiency is maximized. The use of unmanned aerial vehicles (UAVs) in conjunction with sensor networks has emerged as a viable solution for maintaining communication between network nodes. Techniques that use multiple antennas can be applied to minimize energy consumption in wireless sensor networks and assist in communication of such networks with groups of UAVs. The same set of antennas used for communication in UAVs can be used to provide other benefits, such as implementation of an altimeter and a precise positioning system that does not rely on external agents. This work presents a set of techniques for antenna arrays that can improve the efficiency of sensor networks, provide automated and safe control for UAVs and enable efficient interaction between these two systems.

Keywords: Unmanned Aerial Vehicle, Wireless Sensor Networks, MIMO, Antenna Arrays

CONTENTS

LIST OF FIGURES

LIST OF TABLES

Chapter 1

Introduction

Recent advances in electronics and miniaturization have allowed the development of small, low-powered and low-cost devices capable of small range communication, a limited amount of processing and of collecting data about its surroundings. Wireless sensor networks are a collection of such devices, called nodes, organized in a cooperative network environment. They possess various advantages over traditional sensor applications. Due to their low-cost and small size they can be deployed densely and randomly in order to monitor a certain phenomenon, on the other hand, traditional sensors usually require extensive planning in their deployment and, depending on the nature of the phenomenon to be sensed, cannot be placed near it due to their high cost. Wireless sensor networks are usually self contained and capable of organizing the network on the fly. Due to this characteristics these networks are suitable for deployment on harsh environments. Their usage ranges from military applications, such battlefield surveillance and targeting, to health applications, such as automating drug applications in hospitals [1].

However, the tight energy constrain still limits the usage of WSNs as replacing their power source is, usually, prohibitively costly. This has led to extensive research on maximizing energy efficiency on WNS. With most of the energy being used for communication [2], it is important to develop energy aware strategies for all processes involved in exchanging data across the network. Energy efficient protocols for medium access control have been proposed in [3][4]. Energy efficient routing protocols can be found at [5, 6]. Power aware processing for communication has been proposed in [7]. Finally some physical layer alternatives are proposed in [8][9].

The usage of mobile nodes to enhance connectivity and to perform as sinks in WSNs has been proposed in [10]. Mobile nodes are capable of enhancing the self organizing abilities of WSNs since they can replace strategical nodes in order to avoid that a set of nodes remains disconnected from the rest of the network. To perform the roll of mobile nodes a good option is to resort to unmanned aerial vehicles (UAVs). These aircrafts can be employed at harsh environments, since they suffer no interference from the terrain, and they can provide a reliable communication path along the network. However, autonomous UAV relies on its ability to locate itself and to make decisions with respect to its current altitude, position and attitude.

This work explores antenna array techniques in order to provide improved energy efficiency in

WSNs and to allow precise UAV location and control through a radio altimeter and a positioning system that does not rely on external agents. This results in increased interoperability between static WSN nodes and fast moving UAVs acting as mobile nodes. Although these techniques are proposed as a framework for improved WSNs, they can be implemented individually and outside of this context.

The problem of energy efficiency in WSNs is addressed by employing a Cooperative MIMO approach. The technique is detailed and a comparison is made between the proposed scheme and conventional communication schemes employed in WSNs. The interaction between Cooperative MIMO enabled networks and mobile nodes is studied and a movement control algorithm for the UAVs is proposed in order to maintain optimal node distribution and communication along the network.

Antenna array based techniques are proposed in order to enhance the UAVs positioning capabilities. An antenna array based radio and an antenna array based positioning system are proposed in order to make UAVs more reliable and autonomous in harsh or military type environments.

The remainder of this work is divided into four more chapters. Chapter two presents the mathematical background for the proposed techniques, tensor algebra, subspace decomposition and a direction of arrival (DOA) estimation scheme name ESPRIT are introduced. A brief introduction to MIMO systems is also present.

In Chapter three a Cooperative MIMO framework is presented, simulations show that the proposed technique is capable of achieving increased energy efficiency, network connectivity, reduced packet delivery delay and also capable of enhancing the communication between static and mobile nodes in WSNs. The enhanced relationship between static and mobile nodes is also used in order to achieve connectivity in sparse WSNs, by introducing a movements control algorithm.

Chapter four explores the presence of antenna arrays on mobile nodes, namely UAVs, in order to achieve improved location estimation methods. An antenna array based radio altimeter is introduced, the proposed system is capable of mapping the entire ground topology with precision and without relying on mechanical components. A system capable of estimating the attitude and the position of the UAV by employing only an antenna array is also presented and compared to existing techniques.

Finally, conclusions are drawn in Chapter five and proposals for future research are presented.

Chapter 2

Background

The following chapter presents a basic introduction to tensor notation and the basics of tensor algebra. A signal model is derived, in both matrix and tensor representation, to be used in the rest of this work. The ESPRIT parameters estimation algorithm is introduced is both matrix and tensor form. A brief introduction to MIMO systems is also presented is this chapter.

2.1 Tensor Calculus

Tensors can be seen as the extension of matrix notation to dimensions greater than two. Tensors shall be denoted by bold upper case calligraphic variables, an order-R tensor is defined as

$$\boldsymbol{\mathcal{A}} \in \mathbb{C}^{M_1 \times M_2 \times \ldots \times M_R}. \tag{2.1}$$

Tensor $\boldsymbol{\mathcal{A}}$ has R dimensions with each r dimension possessing M_r elements. As shown in Figure 2.1 order-0 tensor can be pictured as a scalar, an order-1 tensor as a vector, an order-2 tensor as a matrix and an order-3 tensor as a cube containing its elements. Higher order tensors cannot be visualized by the human mind but serve as more organized and natural ways to represent data in many applications.

2.1.1 Tensor Unfolding

In order to operate with tensor using well-know linear algebra tools via the application of tensor unfoldings. This operation transforms a tensor of dimension $R \geqslant 2$ into a matrix. The r-mode

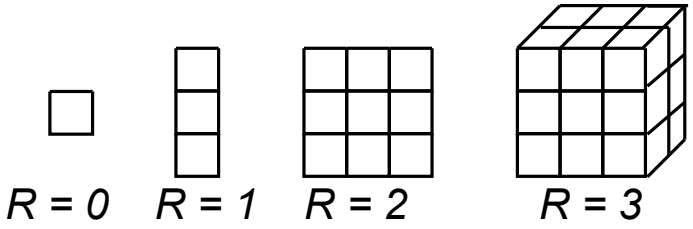

Figure 2.1: Graphical tensor representation

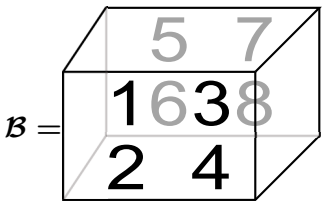

Figure 2.2: Tensor $\mathcal{B} \in \mathbb{R}^{2\times2\times2}$

unfolding of tensor $\mathcal{A}$ is denoted by

$$[\mathcal{A}]_{(r)} \in \mathbb{C}^{M_r \times (M_1 \cdot M_2 \cdot \ldots \cdot M_{r-1} \cdot M_{r+1} \cdot \ldots \cdot M_R).} \tag{2.2}$$

$[\mathcal{A}]_{(r)}$ is a matrix containing the r-mode vectors or r fibers of tensor $\mathcal{A}$ along its rows. A r-mode vector can be obtained by fixing the index of all dimensions other than r and varying the index of the r-th dimension along its range.

The unfoldings of the tensor presented in Figure 2.2 are given by

$$[\mathcal{B}]_{(1)} = \begin{bmatrix} 1 & 3 & 5 & 7 \\ 2 & 4 & 6 & 8 \end{bmatrix}, \tag{2.3}$$

$$[\mathcal{B}]_{(2)} = \begin{bmatrix} 1 & 2 & 5 & 6 \\ 3 & 4 & 7 & 8 \end{bmatrix}, \tag{2.4}$$

$$[\mathcal{B}]_{(3)} = \begin{bmatrix} 1 & 2 & 3 & 4 \\ 5 & 6 & 7 & 8 \end{bmatrix}. \tag{2.5}$$

2.1.2 r-Mode Product

The r-mode product of a tensor $\boldsymbol{\mathcal{A}} \in \mathbb{C}^{M_1 \times M_2 \times \ldots \times M_r}$ and a matrix $\boldsymbol{D} \in \mathbb{C}^{L \times M_r}$ is denote by

$$\boldsymbol{\mathcal{C}} = \boldsymbol{\mathcal{A}} \times_r \boldsymbol{D} \in \mathbb{C}^{M_1 \times M_2 \times \ldots \times L \times \ldots \times M_r}, \tag{2.6}$$

which is equivalent to

$$[\boldsymbol{\mathcal{A}} \times_r \boldsymbol{D}] = \boldsymbol{D} \cdot [\boldsymbol{\mathcal{A}}]_{(r)}. \tag{2.7}$$

Thus, the matrix $\boldsymbol{D}$ must have the same number of columns as the numbers of elements in the r-th dimension of $\boldsymbol{\mathcal{A}}$.

2.2 Data Model

The signal propagation will be modeled as planar wave fronts, as receivers are considered to be located on the far field of the transmitting antennas. Considering d planar wave fronts impinging on a uniform rectangular antenna array containing $M \times M$ elements as displayed on Figure 2.3.

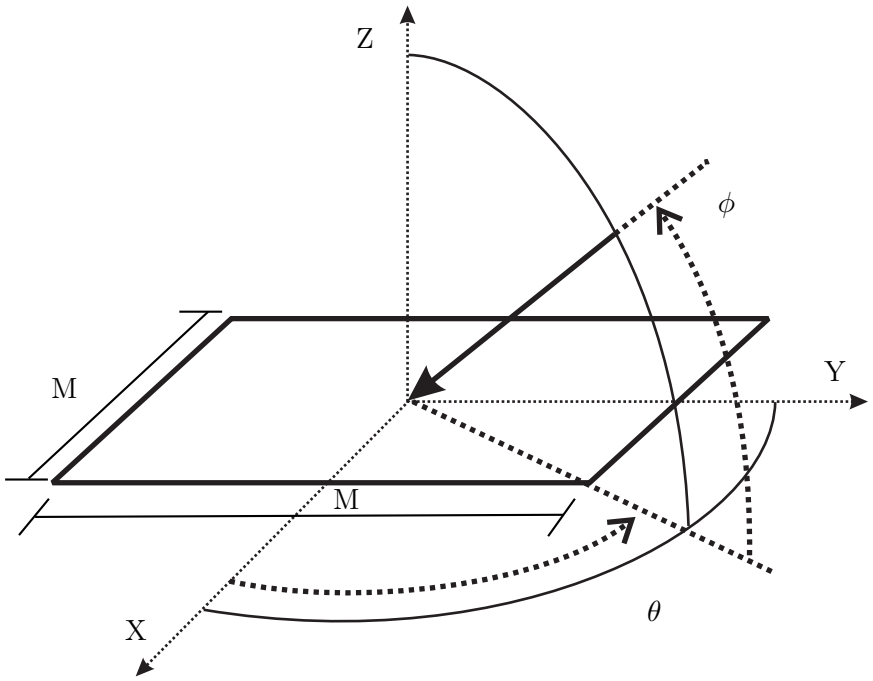

Figure 2.3: Graphical representation of a $M \times M$ URA

Antennas are considered to be omnidirectional and the antenna array calibration is assumed to be perfect, i.e, all antenna elements inflict the same attenuation or phase delay on the received signal. The signal received at the $m_{1,}m_2$ antenna at a given time snapshot t is given by

$$x_{m_1,m_2,t} = \sum_{i=1}^{d} s_i(t) \prod_{r=1}^{R} e^{j\cdot(1-m_r)\cdot\mu_i^{(r)}} + n_{m_1,m_2,t}, \tag{2.8}$$

where j represents the imaginary number $j^2 = -1$, $s_i(t)$ is the complex symbol transmitted by the i-th source at time snapshot t, $n_{m_1,m_2,t}$ is the zero mean additive white Gaussian noise present at antenna m_1, m_2 at time snapshot t. $\mu_i^{(r)}$ represents the spatial frequency of the signal transmitted by the i-th source over the r-th dimension. For example, the spatial frequencies of a signal impinging over the URA presented on Figure 2.3 are given by

$$\mu_i^{(1)} = 2\pi\frac{\Delta}{\lambda}\cos(\theta_i)\sin(\phi_i), \tag{2.9}$$

$$\mu_i^{(2)} = 2\pi\frac{\Delta}{\lambda}\sin(\theta_i)\sin(\phi_i). \tag{2.10}$$

where θ_i and ϕ_i are the azimuth and elevation of arrival of the i-th signal, Δ is the separation between antenna elements and λ is the wavelength of the incoming signal.

2.2.1 Matrix Notation

Let M_r be the size of the r-th dimension, and $M = \prod_{r=1}^{R} M_r$. A steering vector $\boldsymbol{a}_i^{(r)}$ containing the spatial frequencies relate to the i-th source over the r-th dimension can be defined as

$$\boldsymbol{a}_i^{(r)} = \begin{bmatrix} 1 \\ e^{j \cdot \mu_i^{(r)}} \\ \vdots \\ e^{(M_r - 1) \cdot j \cdot \mu_i^{(r)}} \end{bmatrix}, \tag{2.11}$$

an array steering vector for the i-th source can be written as

$$\boldsymbol{a}_i = \boldsymbol{a}_i^{(1)} \otimes \boldsymbol{a}_i^{(2)} \otimes \ldots \otimes \boldsymbol{a}_i^{(r)} \in \mathbb{C}^{M \times 1}, \tag{2.12}$$

an array steering matrix for the r-th dimension can be constructed as

$$\boldsymbol{A}^{(r)} = \left[\boldsymbol{a}_1^{(r)}, \boldsymbol{a}_2^{(r)}, \ldots, \boldsymbol{a}_d^{(r)} \right] \in \mathbb{C}^{M \times d}, \tag{2.13}$$

finally, a total steering matrix can be constructed as the Khatri-Rao product, equivalent to performing a column wise Kronecker product, of the array steering matrix of all dimensions

$$\boldsymbol{A} = \boldsymbol{A}^{(1)} \diamond \boldsymbol{A}^{(2)} \diamond \ldots \diamond \boldsymbol{A}^{(r)} \in \mathbb{C}^{M \times d}. \tag{2.14}$$

With the array steering matrix (2.8) can be rewritten in matrix form as

$$\boldsymbol{X} = \boldsymbol{A} \cdot \boldsymbol{S} + \boldsymbol{N}, \tag{2.15}$$

where the symbol matrix $\boldsymbol{S} \in \mathbb{C}^{d \times N}$, where N is the number of times snapshots taken, contains the symbols $s_i(t)$ transmitted by the d sources. The matrix $\boldsymbol{N} \in \mathbb{C}^{M \times N}$ contains the white Gaussian noise samples. Note that the resulting $\boldsymbol{X}$ matrix contains the measurements of one snapshot stacked along one column, with the snapshots taken along different dimensions stacked along its rows. This results in a matrix of the type

$$\boldsymbol{X} = \begin{bmatrix} x_{1,\ldots,1,1,1} & x_{1,\ldots,1,1,2} & \cdots & x_{1,\ldots,1,1,N} \\ x_{1,\ldots,1,2,1} & x_{1,\ldots,1,2,2} & \cdots & x_{1,\ldots,1,2,N} \\ \vdots & \vdots & \vdots & \vdots \\ x_{1,\ldots,1,M_R,1} & x_{1,\ldots,1,M_R,2} & \cdots & x_{1,\ldots,1,M_R,N} \\ x_{1,\ldots,2,1,1} & x_{1,\ldots,2,1,2} & \cdots & x_{1,\ldots,2,1,N} \\ x_{1,\ldots,2,2,1} & x_{1,\ldots,2,2,2} & \cdots & x_{1,\ldots,2,2,N} \\ \vdots & \vdots & \vdots & \vdots \\ x_{M_1,\ldots,M_{R-1},M_R,1} & x_{M_1,\ldots,M_{R-1},M_R,2} & \cdots & x_{M_1,\ldots,M_{R-1},M_R,N} \end{bmatrix} \in \mathbb{C}^{M \times N}. \tag{2.16}$$

2.2.2 Tensor Notation

The snapshots can be organized in a more natural way by using tensor notation. Instead of stacking the measurements over a matrix we can represent the snapshots over the third dimension of a measurement tensor, making the snapshots of the URA measurements "slices" of the tensor.

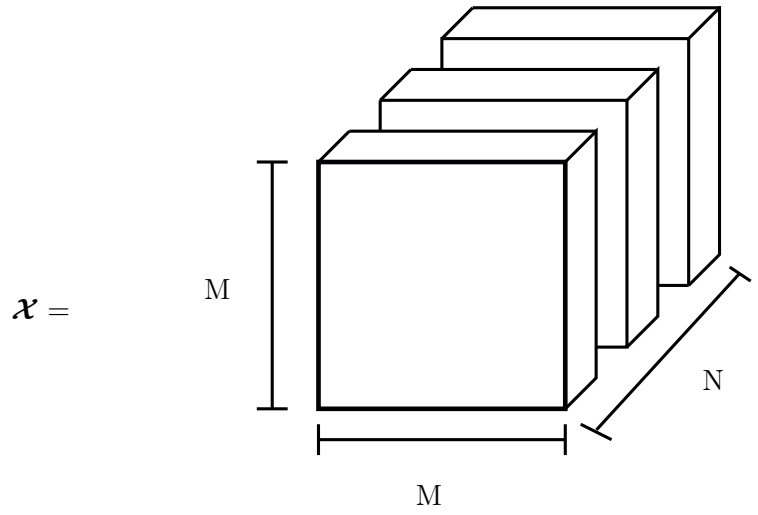

Figure 2.4: Tensor representation of the measurements of the URA

Figure 2.4 shows the tensor representation of the measurement matrix, with the URA geometry being preserved and snapshots being stacked over the third dimension.

A steering tensor for each of the d signal sources can be obtained by the following outer product:

$$\boldsymbol{\mathcal{A}}_i = \boldsymbol{a}_i^{(1)} \circ \boldsymbol{a}_i^{(2)} \circ \ldots \circ \boldsymbol{a}_i^{(r)} \in \mathbb{C}^{M_1 \times M_2 \times \cdots \times M_R}. \tag{2.17}$$

A total array steering tensor can be constructed by concatenating the individual steering tensor for each of the signal sources over the $r+1$ dimension, as it follows

$$\boldsymbol{\mathcal{A}} = [\boldsymbol{\mathcal{A}}_1|_{R+1}\boldsymbol{\mathcal{A}}_2|_{R+1} \ldots |_{R+1}\boldsymbol{\mathcal{A}}_d] \in \mathbb{C}^{M_1 \times M_2 \times \cdots \times M_R \times d}. \tag{2.18}$$

The $|_r$ operator represents the concatenation operation over the r-th dimension.

The measurement tensor $\boldsymbol{\mathcal{X}} \in \mathbb{C}^{M_1 \times M_2 \times \ldots \times M_R \times N}$ can be written very similar to Equation 2.15 as

$$\boldsymbol{\mathcal{X}} = \boldsymbol{\mathcal{A}} \times_R \boldsymbol{S}^{\mathrm{T}} + \boldsymbol{\mathcal{N}}, \in \mathbb{C}^{M_1 \times M_2 \times \ldots \times M_R \times T} \tag{2.19}$$

here $\boldsymbol{\mathcal{N}}$ is the noise tensor and contains the noise samples interfering with the measurements and $\boldsymbol{S}^{\mathrm{T}}$ is the transpose of the symbol matrix. The tensor representation can be transformed into matrix representation and *vice versa* with the following relations

$$\boldsymbol{A} = [\boldsymbol{\mathcal{A}}]^{\mathrm{T}}_{(R+1)}, \tag{2.20}$$

$$\boldsymbol{N} = [\boldsymbol{\mathcal{N}}]^{\mathrm{T}}_{(R+1)}, \tag{2.21}$$

$$\boldsymbol{X} = [\boldsymbol{\mathcal{X}}]^{\mathrm{T}}_{(R+1)}. \tag{2.22}$$

2.3 Matrix Subspace Decomposition

The ESPRIT parameter estimation techniques used through this work are based on subspace decomposition. Matrix subspace decomposition is usually done by applying the Singular Value

Decomposition (SVD). The SVD of the matrix $\boldsymbol{X} \in \mathbb{C}^{M \times N}$ is given by

$$\boldsymbol{X} = \boldsymbol{U}\boldsymbol{\Lambda}\boldsymbol{V}^{\mathrm{H}}, \tag{2.23}$$

where $\boldsymbol{U} \in \mathbb{C}^{M \times M}$ and $\boldsymbol{V}^{N \times N}$ are unitary matrices called the left-singular vectors and right-singular vectors of $\boldsymbol{X}$ and $\boldsymbol{\Lambda} \in \mathbb{C}^{M \times N}$ is pseudo diagonal matrix containing the singular values of $\boldsymbol{X}$. The signal subspace $\boldsymbol{E}_S$ of $\boldsymbol{X}$ can be constructed by selecting only the singular vectors related to the d largest singular values, the remaining singular vectors form the noise subspace $\boldsymbol{E}_N$ of $\boldsymbol{X}$. If the rank d is not known a priori it can be estimated using model order selection schemes such as the ones presented in [11][12].

Equivalently eigenvalue decomposition can be applied on the auto correlation matrix $\boldsymbol{R}_{\boldsymbol{X}\boldsymbol{X}} \in \mathbb{C}^{M \times M}$ of $\boldsymbol{X}$ spanning the same subspace

$$\boldsymbol{R}_{\boldsymbol{X}\boldsymbol{X}} = \frac{1}{N}\boldsymbol{X}\boldsymbol{X}^{\mathrm{H}}, \tag{2.24}$$

$$\boldsymbol{R}_{\boldsymbol{X}\boldsymbol{X}} = \boldsymbol{E}\boldsymbol{\Sigma}\boldsymbol{E}^{\mathrm{H}}, \tag{2.25}$$

where $\boldsymbol{E}$ and $\boldsymbol{\Sigma}$ contains the eigenvectors and eigenvalues of $\boldsymbol{R}_{\boldsymbol{X}\boldsymbol{X}}$. The eigenvectors related to the d largest eigenvalues span the same signal subspace $\boldsymbol{E}_S$ of the single value decomposition. The same holds for the noise subspace of the EVD and left singular vectors of the SVD, $\boldsymbol{E}_N$.

2.4 Tensor Subspace Decomposition

A drawback of the matrix representation is that it is not able to hold the information related to the structure of the receiving array for arrays with more than one dimension. To avoid this loss of information an extension of the SVD can be aplyied for the tensor form of the received signal samples. This extension is know as the Higher Order Singular Values Decomposition (HOSVD) [13] and it can be used to calculate the signal subspace while preserving information about the structure of the sampled data. As with the matrix case the number of signals d must be known or estimated, model order selection for tensors such as the one presented in [12] also offer increased accuracy when compared to matrix based model order selection schemes. The HOSVD of the tensor $\boldsymbol{\mathcal{X}}$ is given by

$$\boldsymbol{\mathcal{X}} = \boldsymbol{\mathcal{S}} \times_1 \boldsymbol{U}_1 \times_2 \boldsymbol{U}_2 \times_3 \ldots \times_R \boldsymbol{U}_{R,} \tag{2.26}$$

where $\boldsymbol{\mathcal{S}} \in \mathbb{C}^{M_1 \times M_2 \times \cdots \times M_R}$ is known as the core tensor and $\boldsymbol{U}_r \in \mathbb{C}^{M_r \times M_r}$ are unitary matrices containing the singular vectors obtained by decomposing the respective unfolding of $\boldsymbol{\mathcal{X}}$. The signal subspace can be constructed by selecting the singular vectors related to the d largest singular values of each of the R decompositions. The tensor representation of the signal subspace $\boldsymbol{\mathcal{E}}_S$ is given by

$$\boldsymbol{\mathcal{E}}_S = \boldsymbol{\mathcal{S}}' \times_1 \boldsymbol{U}'_1 \times_2 \boldsymbol{U}'_2 \times_3 \cdots \times_R \boldsymbol{U}'_{R,}$$

where $\boldsymbol{\mathcal{S}}' \in \mathbb{C}^{d \times d \times \cdots \times d}$, $\boldsymbol{U}'_r \in \mathbb{C}^{M_r \times d}$.

Chapter 3

Cooperative MIMO

In this chapter the Cooperative MIMO technique is introduced and an analysis on the energy-efficiency Cooperative MIMO communications is presented. The interaction between the Cooperative MIMO networks and the mobile nodes is studied, and finally a way of keeping network connectivity by controlling mobile node movement is proposed. The basis for the following chapter can be found in [14].

Energy limitations are the most limiting factor in the utilization of WNSs. Techniques such as multi-hop communication are widely used in order to obtain improved energy efficiency and maximize network life time by spreading energy consumption over different nodes. However care must be taken when applying multi-hop in order to avoid reduced energy efficiency.

When implementing new transmission alternatives a study must be made in order to present a way of automatic selection between standard transmission methods and the new alternative. To this end an efficient routing algorithm must be capable of choosing the optimal path, selecting between standard transmission and the new transmission method based on total energy consumption. It is important that such routing algorithm does not present large differences from algorithms in operation today, so that such transmission method can be implemented with very few changes being necessary.

Apart from standard static node only networks, various implementations of WSNs involving the presence of mobile nodes are emerging. Military applications, such as surveillance using ground WSNs and UAVs and next generation Vehicular ad-hoc Networks (VANETs) for automated traffic are examples of such applications. Usually mobile nodes possess a more powerful hardware and are not subject to the same energy constrains of static nodes. These nodes can serve as sinks or processing centers for these hybrid WSNs. The usually low data rate in relation to the speed at which the mobile nodes move makes the communication between mobile and static nodes prone to errors, requiring retransmissions, this implies in added energy costs for the usually energy limited static nodes. The application of the Cooperative MIMO technique can help minimize retransmissions due to the increased range and data rate achievable, thus resulting in increased life time for these hybrid networks.

Even with extremely high energy efficiency, nodes will eventually have their batteries drained.

Energy consumption may not be distributed equally between the entire network, this may be due to some sensors being more active than others. This might be the case, for instance, of a sensor located between two large clusters of sensors that need to exchange data. This one sensor will be subject to a high energetic demand since it needs to forward information of the others sensors that belong to the adjacent clusters. A WSN placed in a harsh environment might also suffer from losing a porting of its members early in its life time. The result of this reduced number of nodes is a disconnected WSN, where nodes are unable to communicate with far nodes. Even non permanent node failures may lead to a completely inefficient WSN depending on the duration and frequency of such failures. These problems can be mitigated by providing additional communication paths for the network, such as UAVs acting as data sinks for the network as presented in Chapter 4. However, a network might already be equipped with a static sink specific for its purpose, in this case UAVs can be employed to act only as data relays, occupying the space left by the nodes that fail and reestablishing communication across the entire network. These UAVs can be simpler and smaller than their sink counterpart and present no need to make decisions based on the data they are relaying. Such solution has been proposed in [15], this work can be extended by the usage of Cooperative MIMO in conjunction with UAV relays in order to minimize the number of UAVs required and to allow UAVs to travel more freely through the network.

3.1 Wireless Sensor Networks Organization

Wireless sensor networks are at their very principle decentralized, ad hoc and self contained systems. Decentralization, however, does not imply a lack of organization in WSNs, it refers only to the capacity of the network to function properly in the event that any of its components cease to function, i.e, the network does not depend on a single specific element to work. The ad hoc capability implies that a new element can join the network and operate on it without any prior configuration. Being self contained means that wireless sensor networks do not rely on any external system to operate.

With this three characteristics in mind, an analysis can be made on the usual methods of organizing a wireless sensor network. These methods are usually divided into two categories, a peer-to-peer or planar architecture and a cluster based or hierarchical architecture.

In peer-to-peer networks there exists no distinction or separation between members, they often possess exactly the same capabilities and resources. This very loose environment distances itself from usual network organizations and provide a more homogenous and locally autonomous framework. Peer-to-peer network members interact with each other in order to share more than information but also all available resources such as processing power and storage capacity. However, the lack of any “leader” element also means that the task of making decisions as simple as allocating IP addresses to new members can be quite complex.

Cluster based networks, on the other hand, are closer to the conventional network architectures. In cluster based networks the elements are usually divided into two categories: Full Function Devices (FFD) and Reduced Function Devices (RFD). RFDs are elements with limited resources,

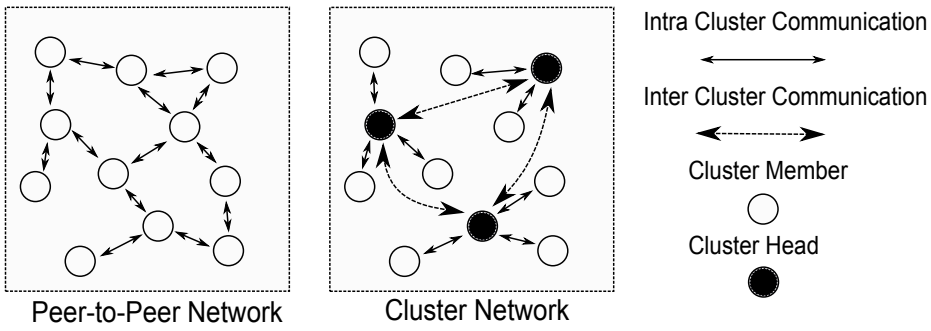

Figure 3.1: Examples of peer-to-peer and cluster networks

usually only possessing a sensing element, a radio for wireless communication and the processing power necessary only to perform the said sensing and forwarding of this captured information. FFDs are more powerful elements, they are responsible for organizing clusters of RFDs, routing and repeating information across the network as well as performing in any network processing necessary, the sensors performing this tasks are known as cluster heads. Although cluster based networks require a more strict type of organization than their peer-to-peer counterpart, they offer a simple way to deal with problems that were arduous on the peer-to-peer networks, as decision making and resource allocating tasks are performed by the FFDs. A cluster network might be comprised entirely of FFDs, which nodes assuming cluster head function depending on various metrics, such as available resources or a pre-configured priority order. In the event that a cluster head ceases to work another FFD will assume its functions.

Regardless of the network organization WSNs are highly cooperative environments with elements working towards a common goal. Due to its highly strict energy budget it is specially important that sensors cooperate when communicating in order to minimize energy consumption and increase network lifetime.

3.2 Energy analysis of conventional techniques

In standard WSNs communication is usually done using either single-hop transmissions or multi-hop transmissions. Single-hop transmissions consist of end to end communications without aid of intermediary nodes while multi-hop transmissions consist of using multiple intermediary nodes as routers in order to convey the necessary data to the destination node.

Figure 3.2 shows an example of single and multi-hop configurations. Note that the multi-hop configuration presents multiple available paths for signal transmission, optimal path selection is problem related to the routing protocol, the reader may refer to [16, 17, 18].

The increased efficiency provided by multi-hop communication is due to the fact that the attenuation suffered by a wireless signal increases exponentially with the distance. However an analysis must be made in order to determine the point where multi-hop ceases to outperform

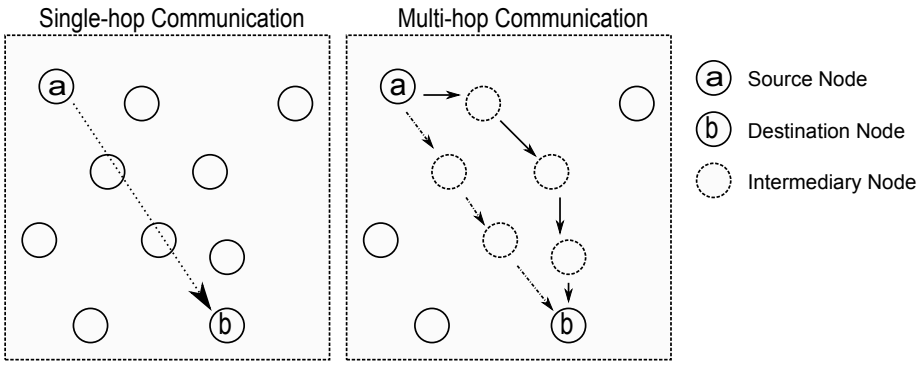

Figure 3.2: Examples of single-hop and multi-hop communication

single-hop. According to the energy consumption model proposed in [19]

$$E_t = \alpha, \tag{3.1}$$

$$E_r = \beta, \tag{3.2}$$

where E_t is the energy necessary for transmitting a single symbol over a certain distance and E_r is the energy necessary for receiving and decoding the given symbol. The parameter α is directly dependent on the distance between the transmitting and receiving nodes and can be written as

$$\alpha = \begin{cases} a + b \cdot d^{\gamma} & ; d_{max} \geq d > d_{min} \\ a + b \cdot d_{min}^{\gamma} & ; d \leqslant d_{min} \end{cases} \tag{3.3}$$

here d_{min} defines the maximum distance that can be reached by setting the transmit power of the transmitting node radio to its minimum configurable value, d_{max} is the maximum reachable distance by setting the transmit power to its highest configurable value, d is the distance between the transmitting and receiving nodes and γ is the path loss coefficient. In order to evaluate the energy efficiency of both techniques we compare a transmission over d_{max} using both techniques. Let $d_{max} = k \cdot d_{min}$ and the path loss coefficient be equal to the free space loss coefficient $\gamma = 2$ and the power necessary for receiving a signal being equivalent to the power necessary for minimal transmission $\beta = a$. In fact receiving is usually more energy demanding than transmitting at low power as seen on table 3.1.

The total energy consumed in a single-hop transmission can be described by using Equations 3.1 and 3.2 as

$$E_r + E_t(d_{max}) = 2a + b \cdot d_{max}^2 = 2a + b \cdot (k \cdot d_{min})^2, \tag{3.4}$$

equivalently, the energy consumed by the multi-hop transmission over k symmetric hops can be written as

$$k \cdot E_r + k \cdot E_t(d_{min}) = k \cdot a + k \cdot (a + b \cdot d_{min}^2) = 2 \cdot k \cdot a + b \cdot k \cdot d_{min}^2. \tag{3.5}$$

From Equations 3.4 and 3.5 we can derive the condition that makes single-hop more energy efficient than multi-hop

$$k \leq \frac{2a}{b \cdot d_{min}^2}. \tag{3.6}$$

Mode	Current
Rx	7.03mA
Tx (-18 dBm)	3.72mA
Tx (-13 dBm)	5.21mA
Tx (-10 dBm)	5.37mA
Tx (-6 dBm)	7.05mA
Tx (-2 dBm)	8.47mA
Tx (0 dBm)	11.57mA
Tx (+3 dBm)	13.77mA
Tx (+4 dBm)	17.37mA
Tx (+5 dBm)	21.48mA
Tx (+10 dBm)	27.01 mA

Table 3.1: Energy consumption for the Mica2 platform

According to [20][21], a condition necessary for minimizing energy consumption in multi-hop is that the hop distance is the same for all hops. For n intermediary nodes place between two nodes separated by a distance D we have the hop distance

$$d_{hop} = \frac{D}{n}, \tag{3.7}$$

replacing 3.7 at 3.5 and taking its derivative with respect to n, the number of hops that minimizes the energy consumption in multi-hop communications can be found

$$n_{opt} = \sqrt{\frac{b}{2a}} \cdot D. \tag{3.8}$$

By replacing 3.8 at 3.7 the optimum hop distance in terms of energy consumption can be written as

$$d_{char} = \sqrt{\frac{2a}{b}}, \tag{3.9}$$

where d_{char} is known as the characteristic distance. Note that d_{char} depends only upon the values of a and b, thus it is a parameter intrinsic to the sensor in question.

Care must be taken when employing the multi-hop approach to avoid reducing energy efficiency by using an unnecessary number of hops. When properly employed the multi-hop approach can lead to significant energy saving in WSNs. However, multi-hopping suffers from some serious disadvantages. Data forwarding is usually done on a best effort delivery way. That means that the transmitting node has no guarantee of the transmitted data reaching its destination, or that it will be delivered within a given time frame. Multi-hop networking can lead to data congestion on nodes that are located between node clusters that generate heavy traffic, this heavy traffic will also result in a high drain of energy resources the in the nodes responsible for forwarding the data. This will result in a high delivery delay and will eventually lead to depletion of energy in these midway nodes, resulting in a disconnected network. Data relaying is usually done in a decode and forward fashion, this can result in a high delay even when there is no network congestion present.

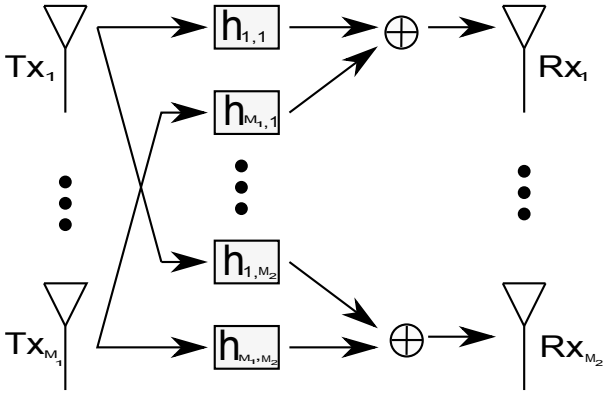

Figure 3.3: Example of a M_1 by M_2 MIMO system

Single-hop transmissions are not affected by network congestion as they are end to end communications, but they require a very high signal power when employed over large distances. If a single sensor is responsible for producing a large amount of data that needs to be transmitted over a large distance, this will lead a very fast depletion of its energy resources. This uneven depletion is highly prejudicial to WSN operation, since replacing individual nodes might be as costly as replacing the entire network. Furthermore single-hop transmissions might be unattainable over large distances due to the limited power at which sensor radios usually operate.

3.3 MIMO Communications

MIMO communications consist of the use of multiple antennas for transmission and reception. The use of multiple antennas is beneficial in various ways. In this work MIMO techniques will be employed in order to achieve spatial multiplexing. Spatial multiplexing is used to transmit parallel bit streams simultaneously over the same frequency. MIMO also results in the array gain, which is the increase of effective received power, due to multiple copies of the signal being received from different antennas.

Consider a sequence of symbols

$$\boldsymbol{s} = [s_1, s_2, ..., s_N], \tag{3.10}$$

that needs to be transmitted over a wireless channel. The channel is assumed to be flat fading, which means that the multipath channel has only one tap, in other words, that the channel impulse response is constant over the frequency. The impulse response between antennas is assumed to be uncorrelated and constant over a transmission period.

The V-BLAST transmission described in [22] is employed for MIMO communications in this work. In a normal transmission at each time slot a single symbol would be transmitted over the channel, in the case of V-BLAST transmission the symbols are grouped into groups the size of the receiving array, in this case, groups of size M_2 , and transmitted over the same time slot.

The received signal at a given receiving antenna x_i at a given time slot can be modeled as

$$x_i = \sum_{k=1}^{M_2} h_{k,i} \cdot s_k + n_i, \tag{3.11}$$

where $h_{k,i}$ represents the complex impulse response of channel between transmit antenna k and receive antenna i and s_k is the symbol transmitted by the k-th antenna. n_i is the noise present at the i-th receiving antenna during sampling. Equation 3.11 can be rewritten in matrix form as

$$x_i = [h_{1,i}, h_{2,i}, ..., h_{M_1,i}] \begin{bmatrix} s_1 \\ s_2 \\ \vdots \\ s_{M_1} \end{bmatrix} + n_i. \tag{3.12}$$

Equivalently a matrix representation for the signals received at all receiving antennas can be written as

$$\begin{bmatrix} x_1 \\ x_2 \\ \vdots \\ x_Q \end{bmatrix} = \begin{bmatrix} h_{1,1} & h_{2,1} & \cdots & h_{M_1,1} \\ h_{1,2} & h_{2,2} & \cdots & h_{M_1,2} \\ \vdots & \vdots & \cdots & \vdots \\ h_{1,M_2} & h_{2,M_2} & \cdots & h_{M_1,M_2} \end{bmatrix} \cdot \begin{bmatrix} s_1 \\ s_2 \\ \vdots \\ s_{M_1} \end{bmatrix} + \begin{bmatrix} n_1 \\ n_2 \\ \vdots \\ n_{M_2} \end{bmatrix}, \tag{3.13}$$

$$\Updownarrow$$

$$\boldsymbol{x} = \boldsymbol{H}\boldsymbol{s} + \boldsymbol{n}, \tag{3.14}$$

The first step necessary in order to estimate the transmitted symbols is to obtain as estimate the channel matrix $\boldsymbol{H}$. An estimate $\hat{\boldsymbol{H}}$ can be obtained by transmitting a set of pilot symbols vectors $\boldsymbol{P} = [\boldsymbol{p}_1, \boldsymbol{p}_2, \ldots, \boldsymbol{p}_U] \in \mathbb{C}^{M_2 \times U}$ where $\boldsymbol{p_i} \in \mathbb{C}^{M_2 \times 1}$ and $U > M_2$

$$\hat{\boldsymbol{H}} = \boldsymbol{X}\boldsymbol{P}^{\dagger}, \tag{3.15}$$

here $\boldsymbol{P}^{\dagger} = \boldsymbol{P}^{\mathrm{H}}(\boldsymbol{P}\boldsymbol{P}^{\mathrm{H}})^{-1}$ is known as the right pseudoinverse of matrix $\boldsymbol{P}$ and the operator $^{\mathrm{H}}$ denotes the conjugate transposition. For a more detailed discussion on tradeoffs and optimal pilot symbol selection for MIMO channel estimation the reader may refer to [23, 24].

Once the channel matrix estimate $\hat{\boldsymbol{H}}$ has been obtained the receiver needs to equalize the received symbols in order to obtain an estimate of the transmitted symbols, various methods exist for performing this equalization, here the Zero Forcing, Minimum Mean Square Error (MMSE) and Maximum Likelihood (ML) methods are anlysed.

The Zero Forcing method consists of finding a matrix $\boldsymbol{W}$ that satisfies $\boldsymbol{W}\boldsymbol{H} = \boldsymbol{I}$, where $\boldsymbol{I}$ is an identity matrix. $\boldsymbol{W}$ is given by

$$\boldsymbol{W} = (\hat{\boldsymbol{H}}^{\mathrm{H}}\hat{\boldsymbol{H}})^{-1}\hat{\boldsymbol{H}}^{\mathrm{H}}. \tag{3.16}$$

As (3.16) shows, the calculation of $\boldsymbol{W}$ is equivalent to calculating the left psesolveudoinverse of $\hat{\boldsymbol{H}}$. An estimate of the transmitted symbols is given by

$$\hat{\boldsymbol{S}} = \boldsymbol{W}\boldsymbol{H}\boldsymbol{S} + \boldsymbol{W}\boldsymbol{N}, \tag{3.17}$$

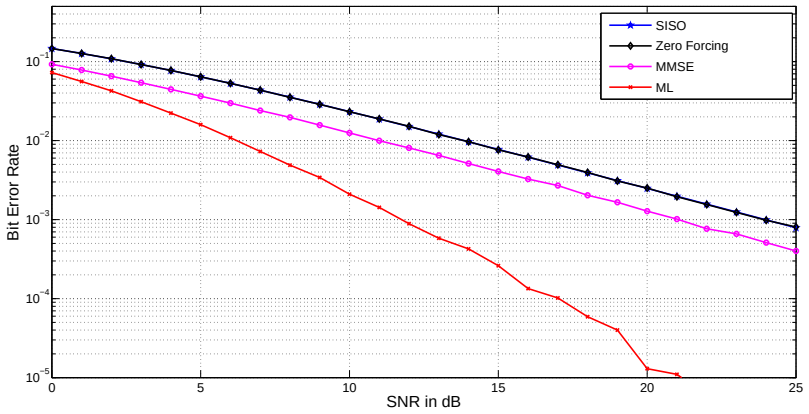

Figure 3.4: Performance comparison between standard SISO systems and 2×2 MIMO systems using Zero Forcing, MMSE and ML equalization

(3.17) shows that depending on the structure of $\boldsymbol{W}$ the received noise might be amplified at equalization, thus degrading the estimate of the transmitted signals.

MMSE equalization tries to solve to problem the of noise amplification by taking into account the noise when calculating the equalizer. MMSE tries to find a matrix $\boldsymbol{W}$ that minimizes the criterion

$$E\left\{[\boldsymbol{W}\boldsymbol{X} - \boldsymbol{S}][\boldsymbol{W}\boldsymbol{X} - \boldsymbol{S}]^{\mathrm{H}}\right\}, \tag{3.18}$$

where $\boldsymbol{W}$ is obtained by

$$\boldsymbol{W} = (\hat{\boldsymbol{H}}^{\mathrm{H}}\hat{\boldsymbol{H}} + N_0\boldsymbol{I})^{-1}\hat{\boldsymbol{H}}^{\mathrm{H}}, \tag{3.19}$$

where N_0 is the power of the received noise. We assume here that N_0 is know, although in practice N_0 needs to be estimated. Notice that in the absence of noise (3.19) reduces to (3.16).

Finally, ML equalization tries to find a matrix $\hat{\boldsymbol{S}}$ such that

$$\mathrm{Err} = \min_{\hat{\boldsymbol{S}}} \left| \boldsymbol{X} - \hat{\boldsymbol{H}}\hat{\boldsymbol{S}} \right|^2. \tag{3.20}$$

The done numerically by testing all possible combinations of $\hat{\boldsymbol{S}}$ and deciding on the one with leads to the minimum Err. Computationally efficient implementations exist for the ML method such as the one presented in [25].

Figure 3.4 shows a comparison between standard SISO systems and a 2×2 MIMO configuration using the equalization methods discussed previously. The ML equalization method is clearly the most efficient in terms of minimizing the bit error rate (BER) of the received bit stream, thus it is the method of choice for the remainder of this work.

3.4 Cooperative MIMO

By introducing a Cooperative MIMO approach the drawbacks of the multi-hop approach can be avoided while still acquiring energy efficient communications. With the fundamentals presented

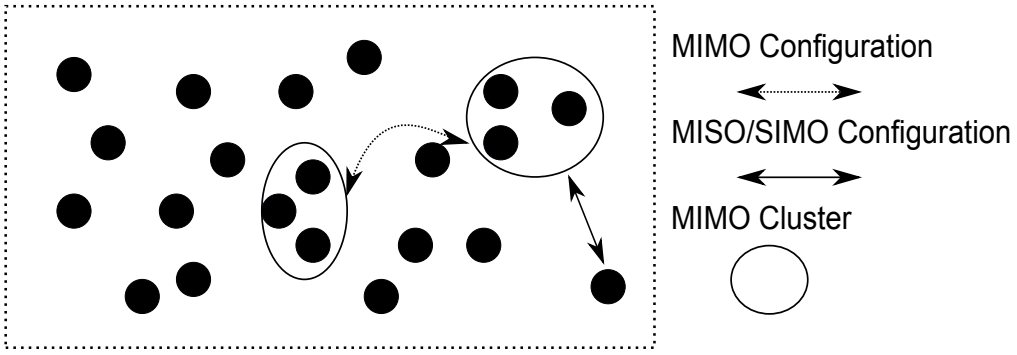

Figure 3.5: Example of a network with MIMO clusters using MIMO, SIMO and MISO configurations

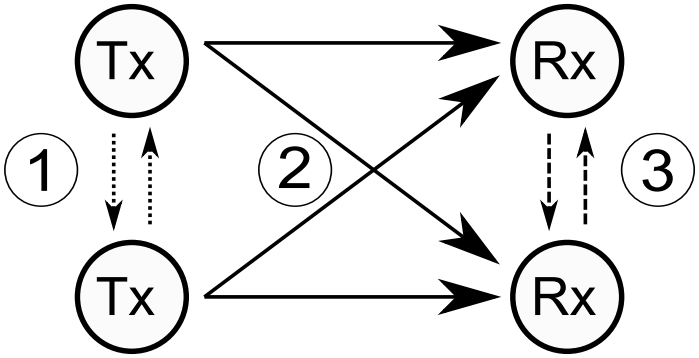

Figure 3.6: Steps involved in Cooperative MIMO communication

on Section 3.3 a reliable, low BER and energy efficient communication can be implemented by taking advantage of the cooperative nature already present on WSNs.

Cooperative MIMO differs from usual MIMO implementations due to the fact that the antenna arrays are not present on the same device, but rather made out of the individual antennas present on each device. By introducing the concept of a MIMO cluster, we create a virtual MIMO device for implementing MIMO communications. A MIMO cluster is completely independent from the cluster concept presented on Section 3.1, and they are interoperable concepts.

In Cooperative MIMO a transmitting node will recruit nearby nodes to aid in data transmission, the destination node will also recruit nearby nodes to aid with the reception and decoding of data. Reception can also be done by a single node, resulting in a SIMO configuration, this can be done to achieve longer distances in communication or to split the energy necessary in long range communication between various nodes. On the other hand, a single node might transmit to a receiving cluster in order to minimize the BER at long range, resulting in a MISO configuration.

When employing cooperative MIMO the transmitted data can come from a single node or various nodes of the transmitting cluster. Figure 3.6 presents the necessary steps in a Cooperative MIMO communication. The first step represented by ① consists of synchronization and exchanging data that needs to be transmitted, if both sensors need to transmit data this exchange is not necessary, as each sensor can transmit its own data. On ② both sensors transmit different symbols

Configuration	Transmissions	Receptions
MIMO (2×2)	6	6
Multi-Hop	3	3
Single Hop	1 (Very High Power)	1

Table 3.2: Amount of transmissions and receptions involved in each communication scheme when nodes are 210 m apart

at the same time slot as stated on Section 3.3. Finally on ③ the receiving sensors exchange the received information in order to decode the received symbol. If the data is destined to only one sensor of the receiving cluster this exchange becomes uni directional. Another option is to exchange only a portion of the received information so that every sensor is responsible for part of the decoding, alleviating the computational burden of a single node.

Cooperative MIMO is capable of reaching large distances without demanding too much power of a single node, also, due to multiple copies of the same signal being received, the BER is considerably smaller at the same SNR, this makes the Cooperative MIMO capable of reaching large distances using much less power than SISO configurations. Cooperative MIMO configurations can lead to even lower BER ratios, and this allow even less power to be used at long range transmissions.

Figure 3.4 shows that a BER of 10^{-3} can be reached with a SNR 10 dB lower using MIMO communication when compared to standard SISO communication. From Table 3.1, going from a 3 dBm transmission to a -13 dBm transmission means that approximately one third as much power is spent to achieve the same BER.

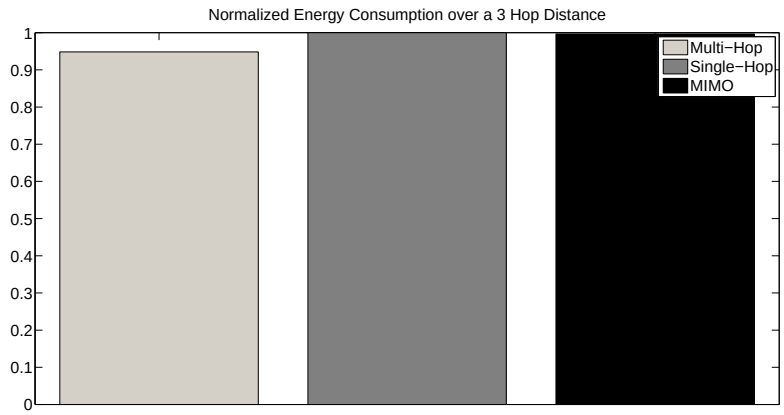

Figure 3.7: Relative energy consumption over 210 m

Table 3.2 presents the amount of transmissions and receptions employed when communicating over 210 m. Figure 3.7 presents a comparison between the energy consumed when communicating using single-hop, multi-hop using 3 hops, and a 2×2 cooperative MIMO. Over 210 m the Cooperative MIMO offers a performance only slightly better than the single-hop and inferior to the multi-hop approach. Its important to notice that even though the difference between MIMO and single-hop was marginal the energy consumption is spread amongst various nodes when using the

Cooperative MIMO, this is highly desirable in WSNs. A comparison must be made when data must travel longer distances, since the increasing amount of receptions necessary starts to become highly demanding energy wise when using multi-hop.

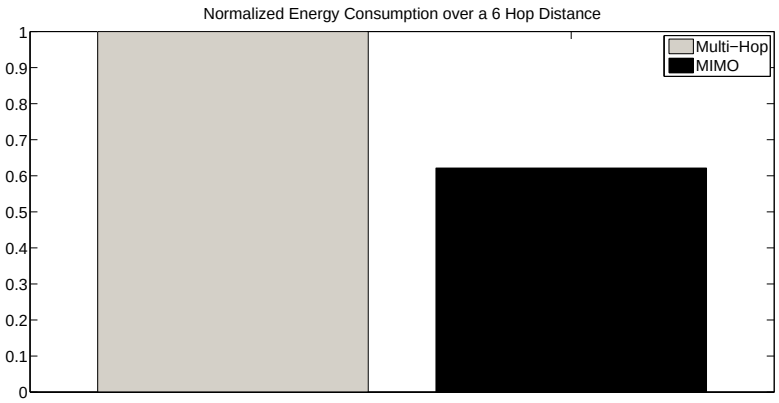

Figure 3.8: Relative energy consumption over 420 m

From Figure 3.8 it is evident the increased efficiency provided by the Cooperative MIMO over large distances.

3.5 Cooperative MIMO Routing

Since Cooperative MIMO starts being beneficial over relatively large distances a selection between using multi-hop and Cooperative MIMO must be made when data needs to be transmitted. Routing can be done either by routing tables, efficient only if the network is fairly stable and suffers little change over time. This methods consists of each individual node assembling routing tables for all possible destinations, this may require a high storage capacity depending on the amount of entries that must kept in said table. Routing may also be done on a on-demand basis with routes being discovered only when needed, this is the case of the Ad hoc On-Demand Distance Vector (AODV) routing protocol. This method is most efficient in dynamical WSNs, where connections change and keeping a large routing table up to date might be unattainable. This method also requires less memory, as paths may be dropped from the list at any time and re acquired when necessary. However the packet exchange involved in constantly trying to find routes may lead to a high overhead, lowering the network performance. The choice of optimal path in either of these routing mechanisms is usually done using the Dijkstra's algorithm. By representing the network as the graph with nodes as vertexes and connections as weighted edges, the algorithm is capable of calculating the optimal path in terms of weight from any vertex to another. Dijkstra's algorithm represents the state of practice in shortest path finding, being used in important routing protocols such as the OSPF (Open Shortest Path First).

Routing in WSNs usually take into account only the number of hops necessary to reach a given target node. In order to take into account Cooperative MIMO, routing algorithms could be

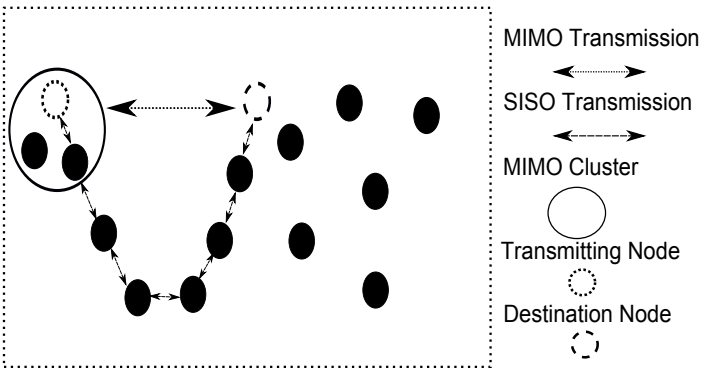

Figure 3.9: Example of more efficient MIMO path

easily adapted to use not the number of hops, but the amount of power involved in transmitting a package over each hop, be it a SISO hop or a MIMO hop, or, if such modification cannot be made, Cooperative MIMO hops can be weighted with a "virtual" number of hops in order to take into account the energy necessary to reach a certain node. This allows networks currently in operation to implement a fast and reliable method of selecting between standard multi-hop transmission and Cooperative MIMO transmission without having to implement complex modifications in their routing algorithms.

Note that in WSNs Cooperative MIMO might be the most efficient method not only when large distances are involved, relatively short distances might be reachable using Cooperative MIMO, while multi-hop transmission could require a large number of hops. Figure 3.9 illustrates this case. Note that, in the absence of intermediary nodes, a cluster of nodes could become completely disconnected from the rest of the network if no Cooperative MIMO was employed, thus, Cooperative MIMO is also capable of diminishing the number of packets dropped due to their destinations being unreachable in the network.

3.6 Simulation Setup for Cooperative MIMO Routing

In order to analyze the performance of an entire network using Cooperative MIMO and compare it with a standard multi-hop only network a set of simulations is performed. When deploying nodes for WSNs which will employ Cooperative MIMO, one needs to ensure the presence of nearby neighbors to aid in data transmission. If careful and planed placement is not possible a statistical guarantee can be achieved by calculating the node density that meets the neighbor requirements for the network.

$$P(c > 1) = (1 - e^{-d\pi r^2})^n, \tag{3.21}$$

here $P(c > 1)$ is the probability that any node has at least one node whiting a r radios, d is the node density and n is the number of nodes in the area. This formula can be easily adjusted to any minimum neighbor number requirement. To guarantee optimal operation for the multi-hop networks an area of 10 km $\times$ 10 km is filled with 5000 nodes, each one presenting a 350 m communication range.

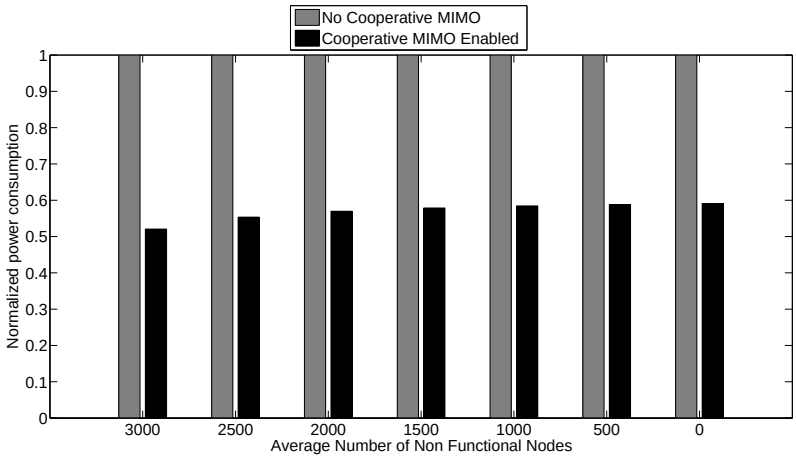

Figure 3.10: Energy consumption comparison between Cooperative MIMO enabled networks and non Cooperative MIMO networks

In order to simulate eventual interference from outside sources, node depletion, node malfunction or nodes being busy with tasks other than communication, several different simulations are performed with random nodes becoming non functional and returning to operation with different rates. The average number of non operational nodes can be easily calculate by applying the Little's law

$$L = F \cdot R, \tag{3.22}$$

where F is the rate of failures, R is the rate of nodes recovering from failure and L gives the average number of non operational nodes at any given moment.

Optimal path selection was made with the Dijkstra's algorithm and the weights used for the edges where based on formulas 3.4 and 3.5.

Packets are generated with a random source and destination, and for the sake of comparison, they are kept between the Cooperative MIMO and non Cooperative MIMO simulations.

3.7 Results and Discussion for Cooperative MIMO Routing

The most important important factor to be observed is the energy efficiency of the network. Figure 3.10 shows the normalized energy consumption comparison between Cooperative MIMO and non Cooperative MIMO networks for the same number of non functional nodes. Energy spent with communications was reduced to roughly 60% of the total energy consumed for transmitting the same amount of data from the same source to the same destination.

Another important factor to be analyzed is the packet delivery delay across the network. Figure 3.11 shows a comparison between packet delivery delay in Cooperative MIMO and non Cooperative MIMO networks. There is a drastic reduction in average delay even for fully operational networks, this is due to the fact that long transmission, which are the ones responsible for the larger portion of the delay, are made using the Cooperative MIMO. Also, packets depend on a smaller number

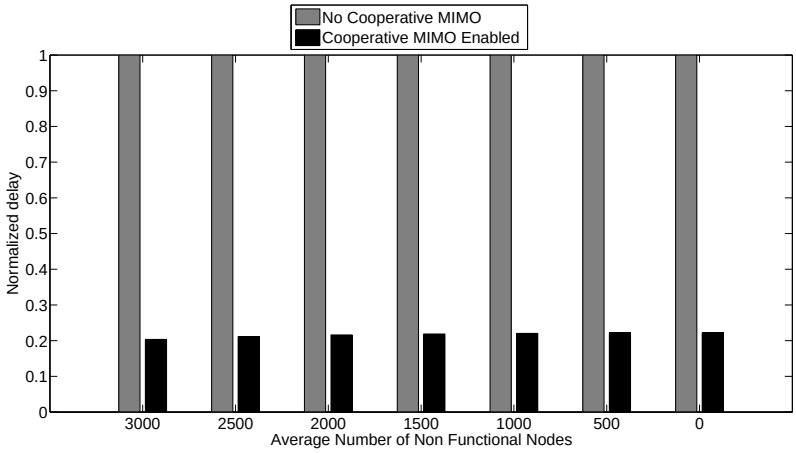

Figure 3.11: Normalized packet delivery delay comparison between Cooperative MIMO networks and non Cooperative MIMO networks

of nodes to be transmitted, hence the probability of a packet being forced to wait for a busy intermediary node is smaller.

Finally, the number of packets dropped due to their destination being unreachable can be compared between both configurations. Figure 3.12 shows the drastic reduction obtained in the number of dropped packets, since Cooperative MIMO is capable of providing increased ranges, the number of unreachable nodes at any given instant is greatly reduced. A more detailed analysis can be made by normalizing the number of packets lost across the different configurations. Figure 3.13 shows that even with a fully operational network, some packets are still dropped when no Cooperative MIMO is used, on the other hand, with the Cooperative MIMO, the number of dropped packets is reduced to almost zero even when 2000 nodes are not operating. This means that for the same area to be covered, the number of nodes necessary to guarantee that the network is fully connected is reduced to $\frac{3}{5}$ of the number necessary for non Cooperative MIMO networks, resulting in a great financial advantage.

3.8 Cooperative MIMO on Hybrid Static-Mobile Sensor Networks

Static sensors on WNSs usually possess radios very limited in power, this results in a very short range. Transmission rates in WSNs are usually very low, with 2000 kb/s being considered a very high rate, and only achievable at small distances between nodes under low SNR. Rates ranging between 80 kb/s - 250 kb/s are typical data rates for WSNs in operation today [26, 27]. At 100 kb/s a 1.5 Mb packet would take approximately 15 seconds to be transmitted. Exchanging audio or video demands large amounts of data to be transmitted with varying quality degrees (depending on the user application), with a 128 kbps audio file having about 1 Mb per minute of recorded audio. This results in a difficult interaction between mobile and static nodes on WSNs as mobile nodes might be forced to move at low speeds in order to avoid breaking the link with the static nodes. Depending on the type of mobile node this might not be possible, UAVs for example cannot

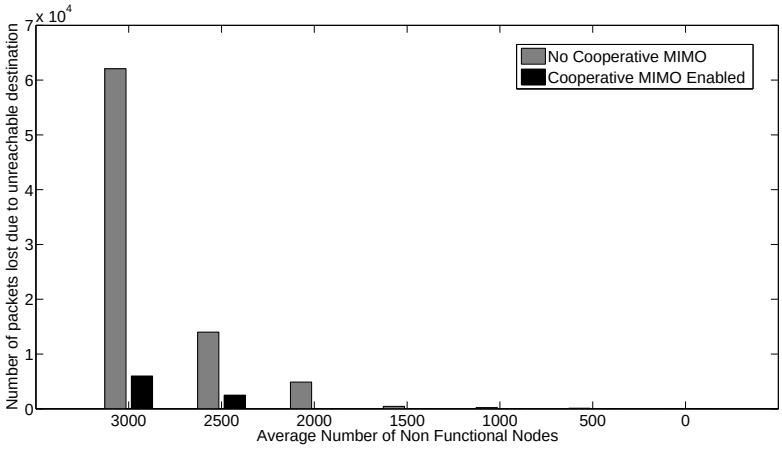

Figure 3.12: Comparison between the number of packets lost due to unreachable destination in Cooperative MIMO and non Cooperative MIMO networks

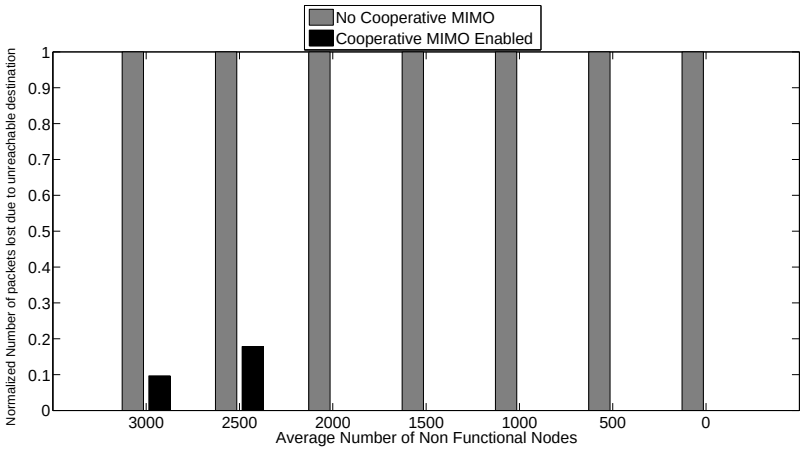

Figure 3.13: Comparison between the normalized number of packets lost due to unreachable destination in Cooperative MIMO and non Cooperative MIMO networks

move at extremely slow speeds. Reducing the velocity of cars in a street would also not be an option on automated traffic. Splitting the data into various packages might not be possible in some cases, for instance a UAV might need the entire data in order to make a decision, taking a photograph or trying to put out a fire for example, or an automated car would need the entire data in order to decide if it should avoid a street closed due to an accident. In [28] an approach involving pre-configured paths for the mobile nodes and the presence of data gathering stations is presented, these requirements can be avoided by employing Cooperative MIMO.

Cooperative MIMO can be used when static nodes need to communicate with mobile elements. As mobile elements are not subject to the same size and complexity constrains as regular sensor nodes, they can be equipped with antennas arrays to allow MIMO communication with a cluster of sensor employing Cooperative MIMO. Using the increased data rate made possible by the V-BLAST method transmission times can be shortened by transmitting multiple parallel symbol streams. Regular transmission times are divided by the amount of nodes employed in the Cooperative MIMO, thus making link breakage less likely to happen during transmission. This will result in less retransmissions and consequently in increased energy efficiency.

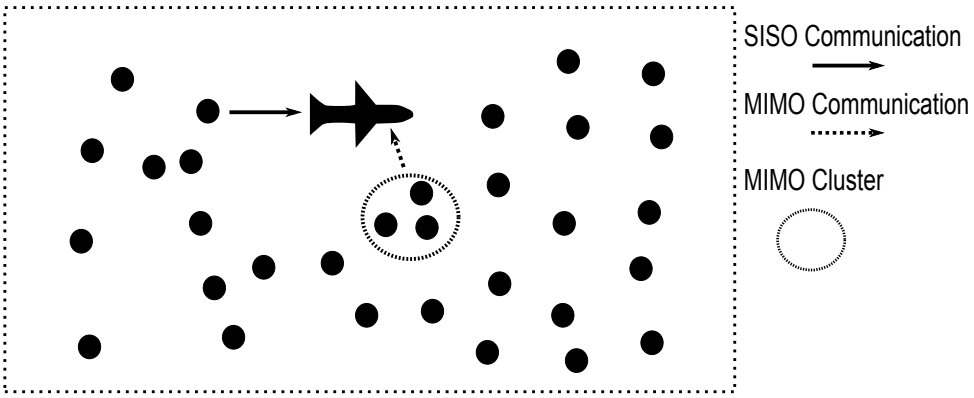

Figure 3.14: Standard and Cooperative MIMO communication between static nodes and a mobile node

3.9 Simulation Setup for Cooperative MIMO in Hybrid Networks

In order to analyze the behavior of Cooperative MIMO in hybrid networks and compare it with networks using only SISO communication, a network composed of static sensor nodes placed at the ground interacting with UAVs acting as sinks is simulated. This scenario is equivalent to a military area under surveillance or to the monitoring of forest areas of difficult access. An area of 10 km $\times$ 10 km is filled with 4500 nodes, each one presenting a 350 m communication range. The nodes' positions are randomly generated. In this scenario, the achieved node density results in an approximately 99.9 % probability of any node having at least another node within a 350 m radius. The relatively small distance between the sensors is needed to guarantee that the MIMO technique is energy efficient. If the sensors were far apart, too much energy would be spent in the communications necessary to share the packets across the nodes step ① in Figure 3.6 due to the

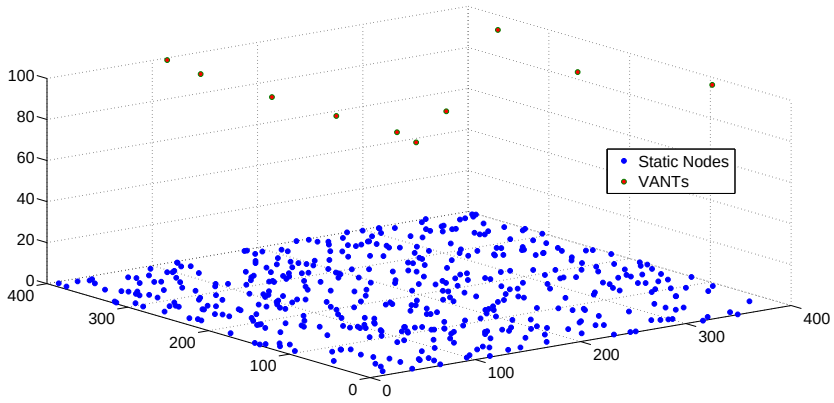

Figure 3.15: Example of simulated scenario

high power needed to transmit over large distances.

Packets are generated across the network with a rate of 4 packets per second and the node generating the packet is chosen following a discrete uniform distribution. The high packet generation rate is chosen to guarantee that the network always presents a packet to be transmitted to each UAV.

The packet transmission priority follows the order of arrival, the older the packet the highest transmission priority is assigned to it. Ten UAVs are distributed in the area with their initial positions randomly chosen using a uniform distribution process. These nodes move according to the Random Way Point (RWP) mobility model and for each way point a random speed is chosen between 70 km/h and 100 km/h.

Figure 3.15 presents the simulated scenario. The dots on the bottom of the figure represent the static sensor nodes on the ground, while the slightly bigger ones on the top represent the UAVs.

The transmission time of a packet (the required time window to transmit a packet) varies from 1 to 15 seconds. The transmission time is composed of the initial handshake process, actual data relay, and the final ACK from the UAVs.

The maximum communication distance between a UAV and a MIMO cluster is 550 m. If the distance is larger than this value at any moment during communication, it is considered that the packet failed to be delivered, since at long distances the BER will be too high. The node will try to retransmit this packet as soon as a UAV is available again with a priority related to the moment it was generated on the network. Each simulation runs for a total of 3600 seconds. For each simulation the number of packets successfully transmitted to the UAVs is measured as well as the number of failed transmissions, i.e. packets that are not delivered. Simulation parameters such as the positions of nodes and movements of UAVs, packet generation time and destination are kept the same across all simulations so as to preserve the same scenario for the sake of comparisons between the obtained results.

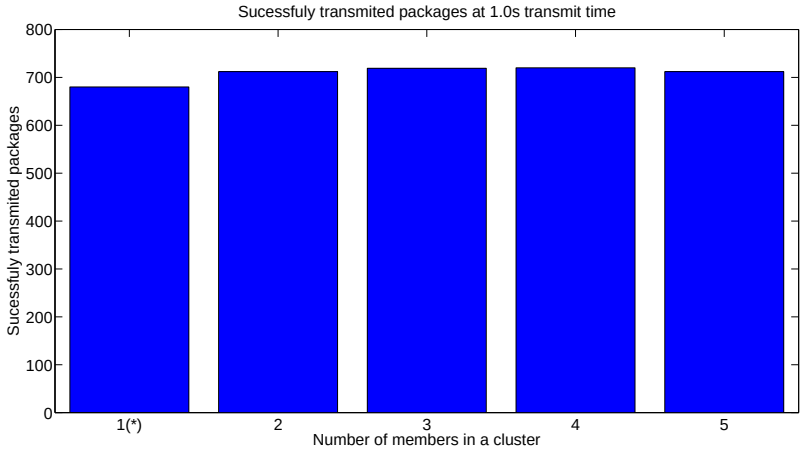

Figure 3.16: Successfully transmitted packages at 1 s transmission time

Figure 3.17: Failed transmissions at 1 s transmission time

3.10 Results and Discussion for Cooperative MIMO in Hybrid Networks

Throughout this section results related to networks where no Cooperative MIMO is employed are shown as 1(*). The first set of results analyzed are the ones obtained at very short transmission times. This set of results is specially import in order to ensure that Cooperative MIMO does not negatively impact the network when only short transmission times are necessary.

Figure 3.16 shows a comparison concerning the numbers of successfully transmitted packets versus the amount of nodes in a MIMO cluster. Due to the very short time window required to perform a transmission, all the packets generated across the network can be successfully transmitted, so the throughput increase is only marginal. It is import to notice that the usage of the Cooperative MIMO does not cause any negative impact on network throughput.

Figure 3.17 shows that even though the throughput presents no significant difference the number of failed transmissions can be minimized by employing the Cooperative MIMO technique. This

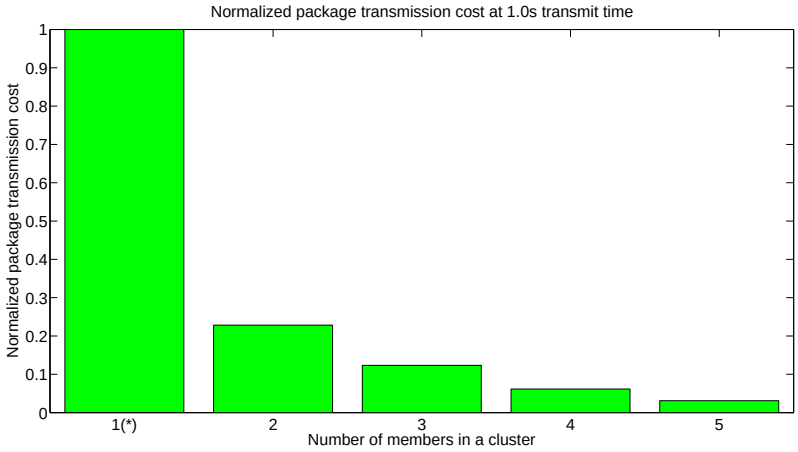

Figure 3.18: Normalized transmission cost at 1 s transmission time

has a direct impact in energy efficiency, as a failed transmission means that energy was effectively wasted by the transmitting nodes.

It is important to define a metric to measure the efficiency in data transmission in order to compare the efficiency provided by the different configurations. The metric of choice in this section is defined as

$$Cost = \frac{Failed\,Transmissions}{Successful\,Transmissions}$$

Figure 3.18 shows that even for fast transmissions the Cooperative MIMO reduces the transmission cost to about 20% of the case with no Cooperative MIMO. This result directly impacts the energy savings across the entire network as, for most WSNs, the communication is the most expensive task in terms of energy consumption. This implies in increased network lifetime without reducing the amount of transmitted data.

Now comes the discussion concerning the impact of Cooperative MIMO on transmissions that require longer time windows to be performed. In this case a link has to be maintained for a long time so that data can be successfully transmitted. The results for the case in which 7 seconds are needed for each transmission are presented in Figures 3.19, 3.20 and 3.21. The cost is reduced to 11% when compared to the case where no Cooperative MIMO is used and the throughput is almost doubled by using two nodes working with the Cooperative MIMO. This allows twice as much data to be transmitted at a much lower energy cost than what would be possible in a non-cooperative network. Finally, for the case in which 15 seconds are needed to transmit a packet, the results are shown in Figures 3.22, 3.23 and 3.24. In this case transmission without the use of Cooperative MIMO is practically impossible, and a larger number of cluster members is necessary to achieve good throughput and cost of transmission on the network. The results show that the technique allows the network to function at costs approximately 12 times lower with 4 members on each cluster. This means that it allows networks with very low transmission rates to transmit to mobile nodes moving at considerably high speeds.

Besides the question of successful transmissions it is important to investigate the possible

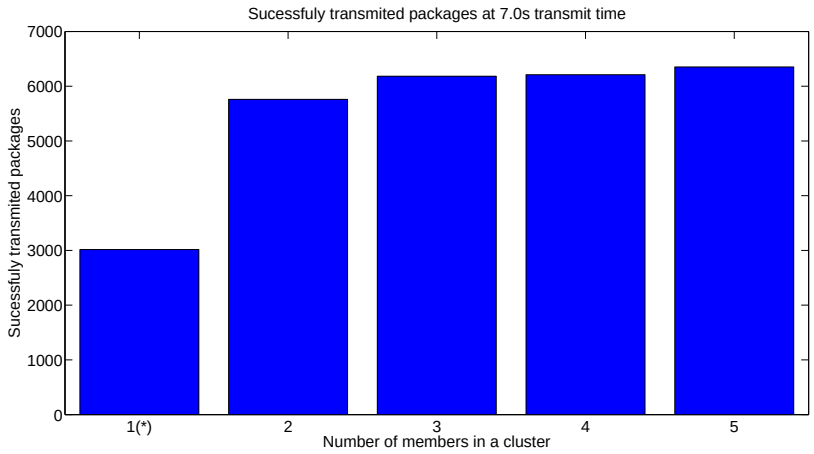

Figure 3.19: Successfully transmitted packages at 7 s transmission time

Figure 3.20: Failed transmissions at 7 s transmission time

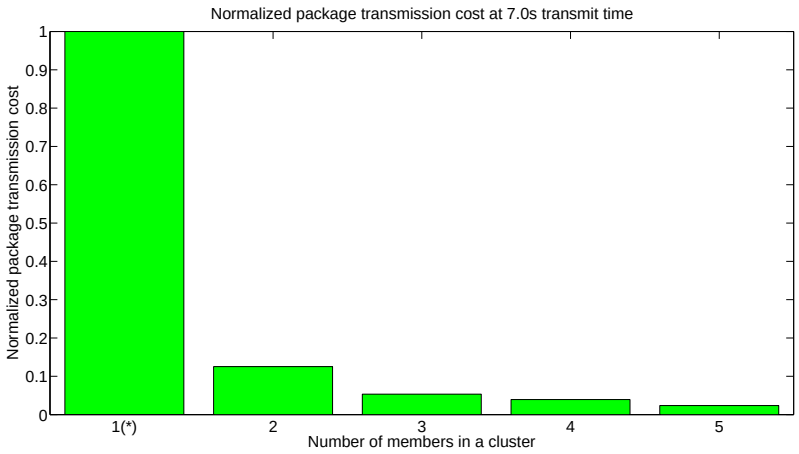

Figure 3.21: Normalized transmission cost at 7 s transmission time

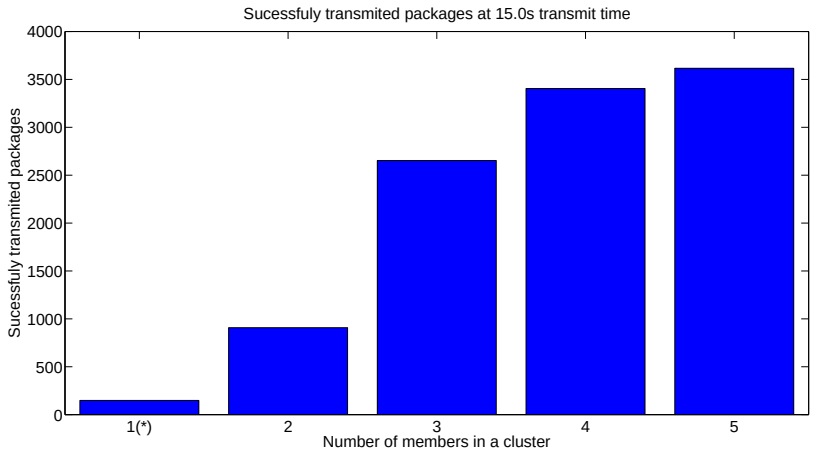

Figure 3.22: Successfully transmitted packages at 15 s transmission time

Figure 3.23: Failed transmissions at 15 s transmission time

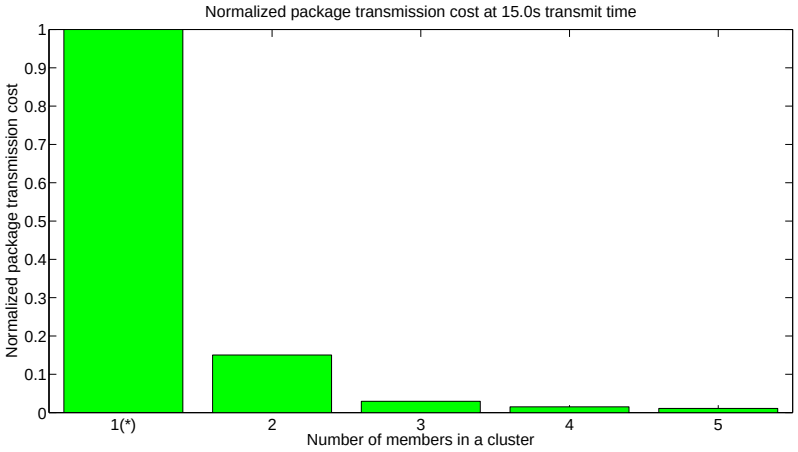

Figure 3.24: Normalized transmission cost at 15 s transmission time

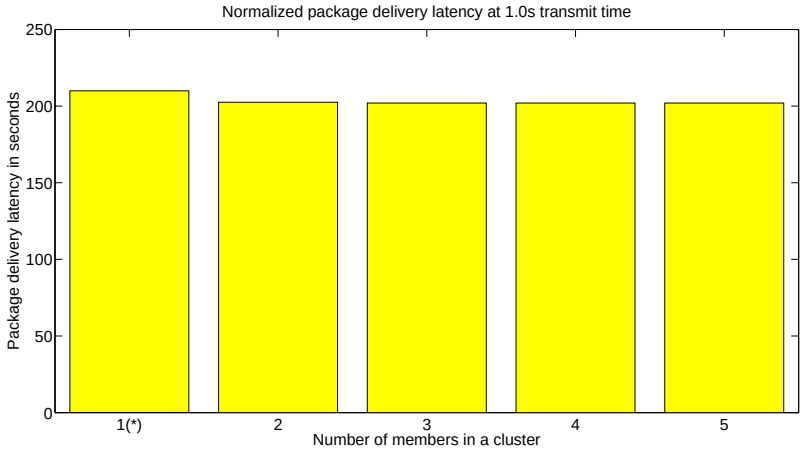

Figure 3.25: Delay at 1 s transmission time

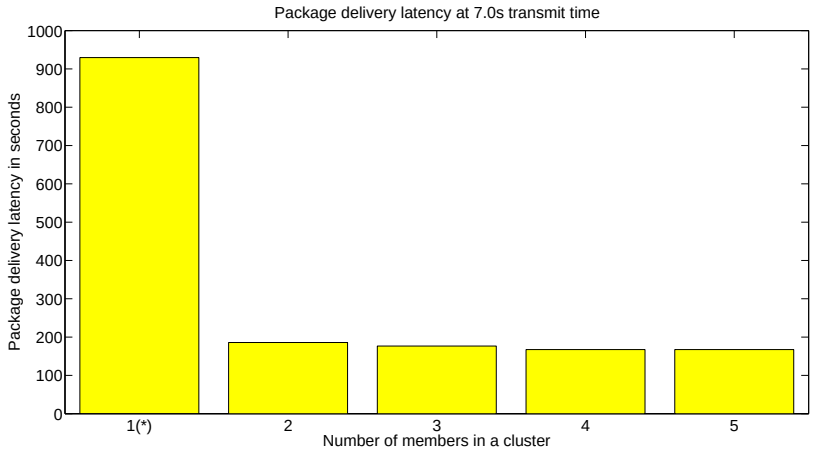

Figure 3.26: Delay at 7 s transmission time

increase in latency across the network, since the packets need to be spread among the nodes involved in the Cooperative MIMO before they can be transmitted to the UAVs. Figures 3.25, 3.26 and 3.27 show that this is not the case because, if the Cooperative MIMO is not used, the amount of retransmissions needed results in a higher latency than that caused by spreading the packets to perform the communication using MIMO.

The delay comparisons presented in Figures 3.25, 3.26 and 3.27 represents the end to end delay, which is the elapsed time between the generation of a packet in the network and the time of this packet's arrival at its destination node, i.e., any UAV. This measure includes the time waiting for retransmission, in case of transmission failure, and also the time for sensor nodes synchronization when using cooperative MIMO configurations.

At very short transmission time windows, a very small positive effect on the delay is observed, since failed transmissions do not occupy the UAVs long enough to have a significant impact on the average network delay. However, for longer transmission time windows, there is a significant positive effect, since failed transmissions will keep the UAVs occupied for longer time periods, thus

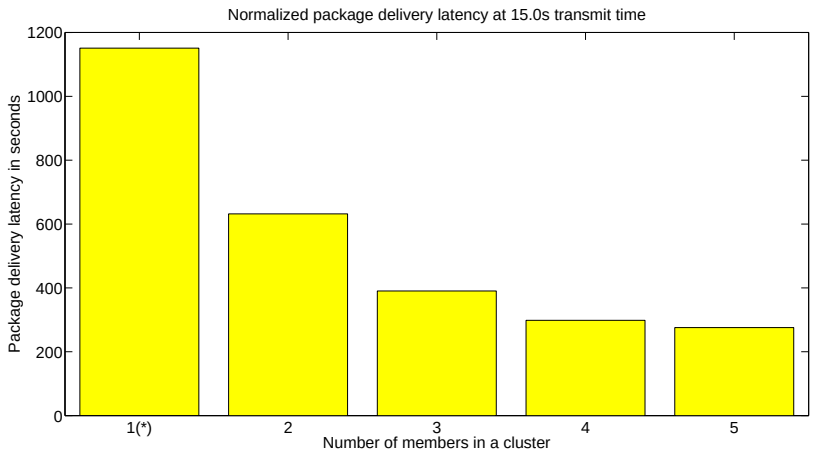

Figure 3.27: Delay at 15 s transmission time

Number of Members in a MIMO Cluster	Required Transmission Time in Seconds		
	1	7	15
1	100%	100%	100%
2	25.69%	14.09%	16.91%
3	15.42%	6.67%	3.67%
4	8.47%	5.40%	2.06%
5	4.67%	3.53%	1.63%

Table 3.3: Comparison between transmission costs for all configurations

making packets wait longer for opportunities to be transmitted.

Finally, it is crucial to analyze the energy consumption of the different setups. Table 3.3 shows that reducing the number of retransmissions comprehensively outweighs the extra energy necessary to spread the packet among the cluster members in the Cooperative MIMO configurations. As the transmission in non-cooperative networks is always the most expensive in terms of cost, it represents the standard cost to which all other configurations are compared. In Table 3.3 the results for the transmission times are presented over the columns and cell values represent the relative transmission cost compared to the case of non-cooperative networks. Energy consumption data is based on the Berkley MICA2 Mote figures presented on Table 3.1.

The results presented in Table 3.3 show that even for short transmission times it is possible to achieve energy efficiency four times larger with the usage of only two nodes on the MIMO cluster. The increase in energy efficiency becomes less noticeable as the number of member nodes grow: the more members in a cluster the less effective it is to add more members. The extra energy efficiency attained might not compensate the extra complexity necessary for implementing the MIMO transmission over a large number of nodes, or the extra number of nodes that need to be added to a network so that the node density is enough to produce clusters with a large number of

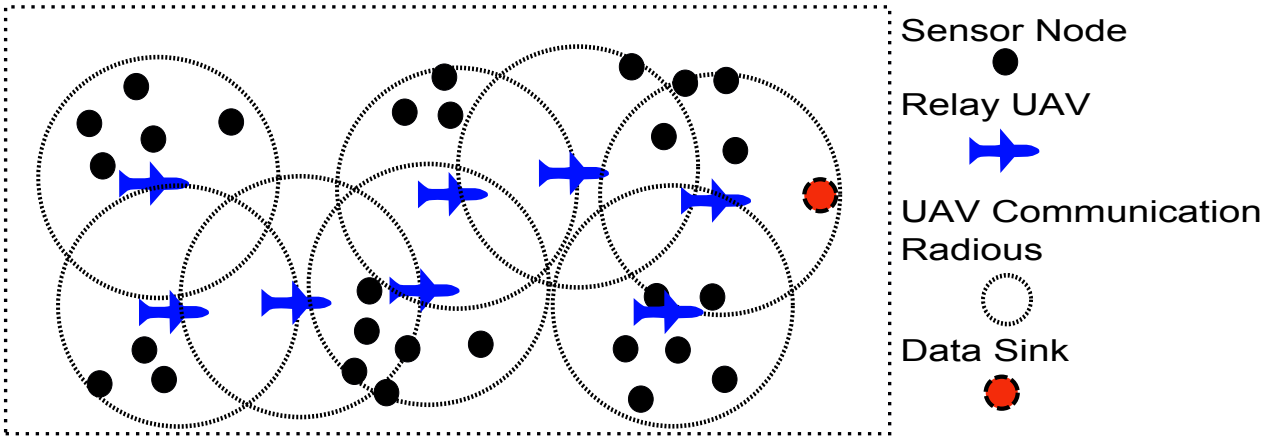

Figure 3.28: UAV Relay Network with no Cooperative MIMO

members. This compromise must be analyzed and is specific for each system requirement.

3.11 Cooperative MIMO and UAV Relays

The approach proposed on [15] considers the node islands only as data generators. The data travels entirely through the network formed by the UAVs. This requires very strict movement from UAVs, as they must remain connected to each other at all times in order to allow data from nodes located far from the sink to be collected. Therefore the number of UAVs necessary for this techniques becomes very large as the area covered by the WSN grows.

Moreover, the UAVs must travel very close to the node islands in order to be able to acquire their information, since the ranges at which a static node is capable of transmitting is extremely limited. A possible solution for minimizing the number of UAVs and allowing UAVs to travel more freely around the network is to implement the Cooperative MIMO technique presented on Chapter 3. The increased range granted by the Cooperative MIMO allows node islands to act not only as data generators but also as static data relays across the network. This results in increased connectivity, allowing the network to function without the necessity of a large number of UAVs.

Figures 3.28 and 3.29 illustrate these differences.

3.12 Moment Control Algorithm

On [15] a movement control algorithm is proposed in order to keep UAVs connected and thus capable of acting as the data transmission backbone of the WSN. The proposed algorithm is based on the received signal strength indicator (RSSI), and states that a UAV will move toward another UAV if it is its only current connection, a relative degree of attraction is made inverse to the received RSSI, the lower the received signal the more inclined to move towards its last connection a UAV is. In the case that the last connection breaks, the UAV will move towards the last known location of its last UAV neighbor.

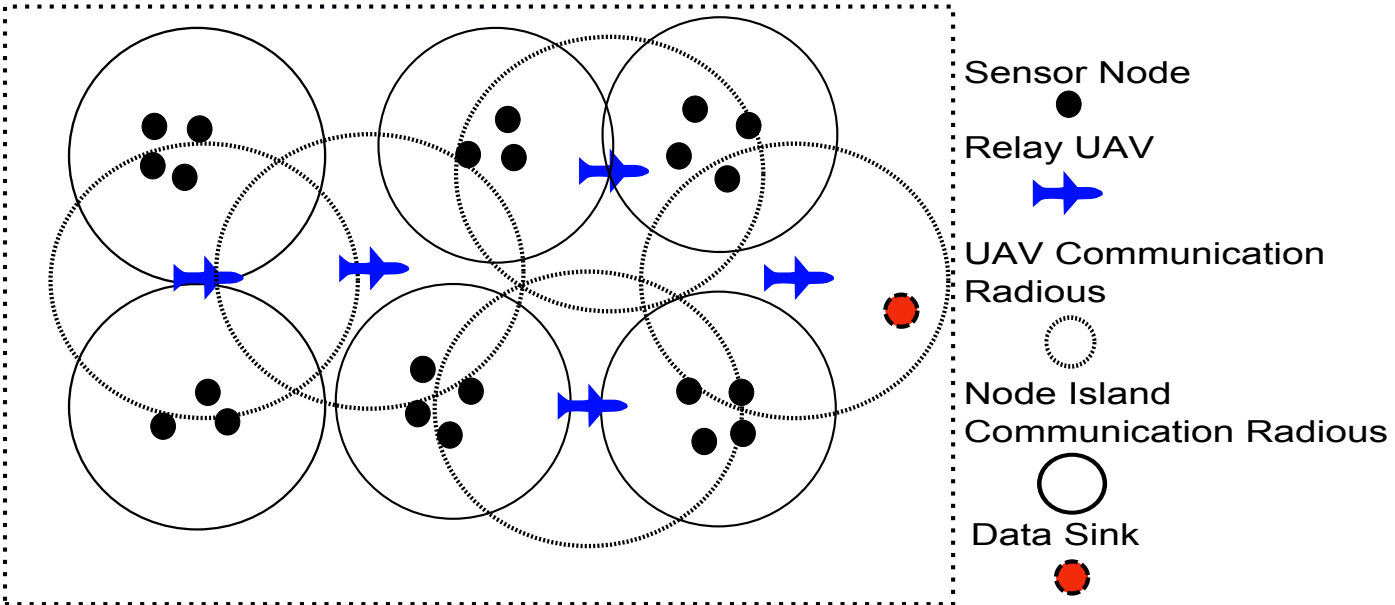

Figure 3.29: UAV Relay Network using Cooperative MIMO

A careful analysis will show that this algorithm must be adapted in order to perform correctly when node islands are treated as data relays. The reason for the adaptation is to avoid that UAVs become "stuck" around a node island whose communication range is short. If a node island is the last of the UAVs connection it will try to keep the connection alive, but since the range of the island communication is very short if a small number of nodes is present to participate in the Cooperative MIMO, the UAV will have its movement limited by the range of the node island. These will effectively turn mobile nodes into semi-static nodes, since their movement will be subject to very harsh constrains. The end result is that UAVs are prone to concentrate around islands with a shorter range, resulting in more nodes disconnected from the sync.

To address this problem a second degree of attraction can be implemented. This second degree of attraction is implemenedt as a probability that a UAV will move towards its last connecting neighbor, be it a node island or another UAV. Said probability is defined as

$$\rho = \frac{n_{max}}{d_{max}}, \tag{3.23}$$

here n_{max} is the maximum communication range of the UAV whose attraction is to be calculated and d_{max} is the maximum communication range of the element to which the UAV will move towards, a island of sensors or another UAV. In case the link is broken the same probability is used to decide if the UAV will move towards the last known location of its last neighbor.

This results is that, when a UAV is connected to nodes that have very short communication ranges, it moves more freely around the node, moving away from the group of nodes at a smaller pace, and eventually drifting a little beyond the maximum communication range. In contrast, when the UAV is connected to a group of nodes that has a large communication range, its movement is adapted to more actively try to keep the link alive and avoid that it breaks. This adaptation prevents the UAVs from having their movement restricted to a very small area around static nodes

that have too short communication range, but it allows keeping connections with nodes that can work as data relays more efficiently.

This allows Cooperative MIMO and movement control to coexist over the same network, as the concentration of UAVs over a certain point depends on the maximum communication range of the node islands, which is directed related to the number of MIMO members in a specific configuration.

3.13 Simulation Setup for Cooperative MIMO and UAV Relays

For the simulation 14, separate node islands are placed in an area of 10×10 m^2. These islands are set so that they are in average 3000 m apart from each other. The UAVs are randomly distributed in the scenario at the beginning of each simulation run, and they follow the random waypoint (RWP) mobility model. The average speed of the UAVs is 85 km / h. A base station is placed at the center of the simulation scenario acting as the sink destination of the data sent by the sensor nodes. Each simulation runs for 3600 seconds. Cooperative MIMO configurations vary from a standard SISO configurations, allowing a maximum communication distance between nodes and UAVs of 350 m, up to 7 cooperating nodes, allowing a communication to a distance of 2450 m. The UAVs communication range is 2450 m.

3.14 Results and Discussion for Cooperative MIMO and UAV Relays

In the simulations the number of nodes disconnected from the sink across different Cooperative MIMO configurations is measured. Energy consumption is an important parameter, the increase energy efficiency of Cooperative MIMO has been demonstrated in previous chapters.

The behavior these sparse networks when no Cooperative MIMO is used needs to be analyzed in order to set the standard to which Cooperative MIMO enabled networks will be compared. In such networks the only tool available for increasing network connectivity is to use a large number of UAVs. Figure 3.30 shows that increasing the number of UAVs that act as relays results only in a marginal effect on average node connectivity. Since, without Cooperative MIMO, nodes have extremely limited communication they depend on UAVs to establish a relay chain from their location to the sink. When UAVs follow a random movement pattern, such as the RWP, these connections will not be established often and will not remain stable for long periods.

Figure 3.31 presents the average connectivity when Cooperative MIMO is employed and only 8 UAVs are present to act as relays. The results show that a degree of connectivity previously unobtainable even with 40 UAVs can be achieved by means of the Cooperative MIMO technique. Considering the improvement presented in Section 3.12, in which the islands of nodes are able to act as relays over larger distances due to the usage of Cooperative MIMO, an important improvement can be noticed in the network as a whole. Nodes that are located far from the sink can now communicate using a combination of UAVs and intermediary groups of sensor nodes and no longer

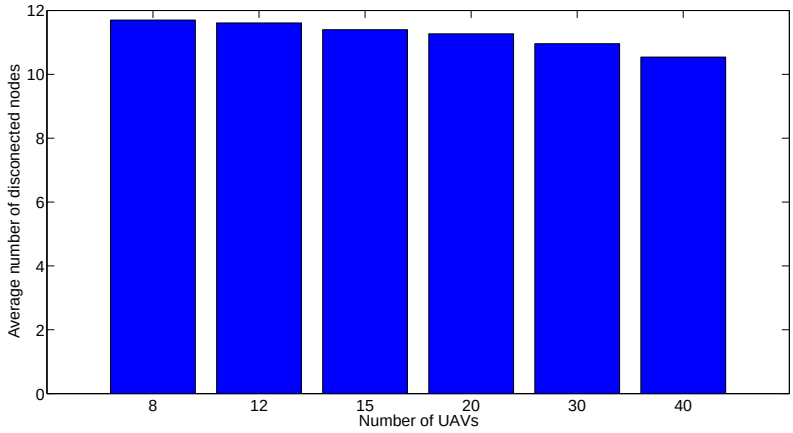

Figure 3.30: Average number of nodes disconnected from the sink in relation to the number of UAVs.

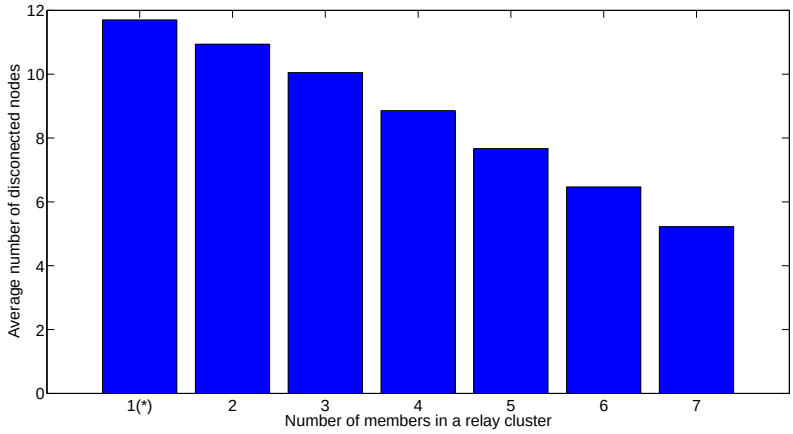

Figure 3.31: Average number of nodes disconnected from the sink in relation to the increasing numbers nodes in a Cooperative MIMO cluster. 8 UAVs are avaliable.

have a great dependency on the UAVs movement pattern. This means that a node that has a data packet that needs to be transmitted to the sink no longer has to wait for a set of UAVs to properly align and provide a path towards the destination; this results in a decreasing latency across the network, especially for nodes located far from the sink. Figure 3.32 shows how the delay drops in relation to an increase in the number of cooperating nodes in the MIMO clusters that are formed in each island of nodes.

The option of increasing the number of UAVs to help connectivity should not be discarded, significant improvements can be obtained when the number of UAVs is increased in Cooperative MIMO enabled networks. Figure 3.33 shows the results of the average number of nodes disconnected from the sink for a varying number of MIMO cluster members when 20 UAVs are distributed over the area. Note there is a significant increase in connectivity when compared with the results presented on 3.31 when only 8 UAVs are present.

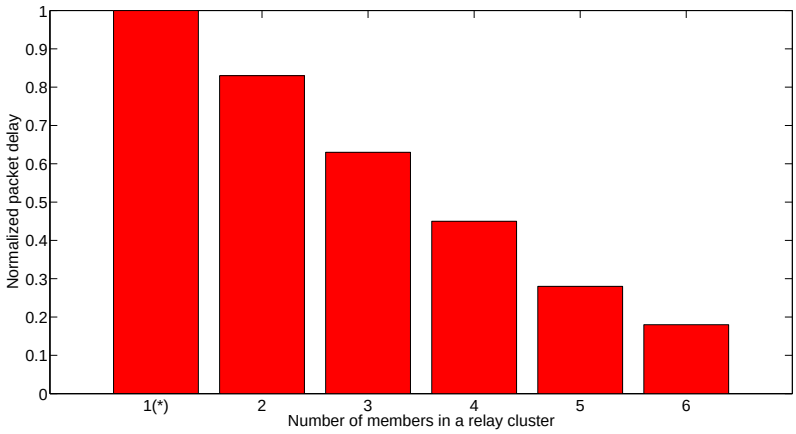

Figure 3.32: Normalized delay in relation to the increasing numbers of MIMO cooperating nodes

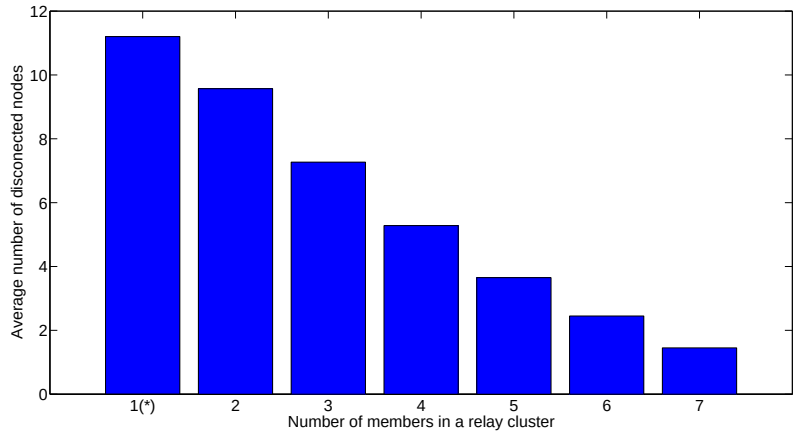

Figure 3.33: Average number of nodes disconnected from the sink in relation to the increasing numbers nodes in a Cooperative MIMO cluster. 20 UAVs are avaliable.

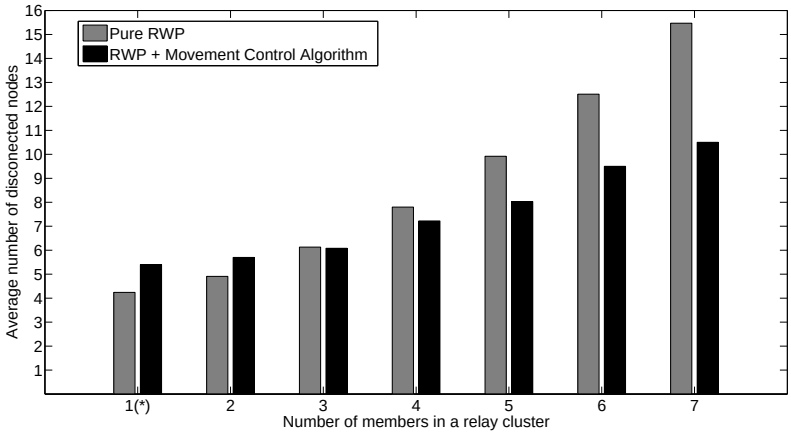

Figure 3.34: Average number of neighbors in relation to the increasing numbers of MIMO cooperating nodes and movement pattern

Another problem minimized is the probability of link breakage, as a smaller number of mobile participants (UAVs) is necessary, since the islands of static nodes also serve as long range relays, it is less likely that the connection will be broken before the node that originally transmitted the package can get a confirmation of its delivery. It is important to notice that, with the values established in the simulation setup, the islands of nodes are not able to connect among them, they only relay messages from and to UAVs that are connected to them. It is also important to highlight that the increased communication distance obtained with the Cooperative MIMO allows the UAVs to maneuver over a much larger area without breaking these connections.

The impact of the movement control adaptation proposed on 3.12 to keep UAVs from breaking connection is now analyzed. Figure 3.34 presents the average number of neighbors, mobile or islands, connected to a UAV during the simulations in which 8 UAVs are covering the area moving according to a Pure RWP and the controlled RWP proposed on [15].

The results show that at short communication ranges (no Cooperative MIMO or Cooperative MIMO clusters with few members) the movement control helps increasing the overall network connectivity. However, as the number of MIMO cluster member increases, and consequently the communication range, the algorithm starts to negatively impact the network connectivity. This is due to the fact that it may lead to eventual deadlocks in which the UAVs become stuck in given locations, or to one neighbor that is disconnected from the rest of the network. If two UAVs are connected only to each other, they will start to move towards each other when the RSSI starts to get weak, once close enough they will start to move randomly again, if no other connection is made the signal will eventually drop again and the process will be repeated, keeping both UAVs connected to each other but disconnected from the rest of the network. The same may happen to a UAV in relation to node islands that have longer communication ranges. In this case the UAVs risks becoming “anchored” to a given island. On the other hand, the UAVs moving with a Pure RWP can benefit from the longer communication ranges of the node islands by being able to connect to other UAVs farther way, without the risk of the same deadlock mentioned above.

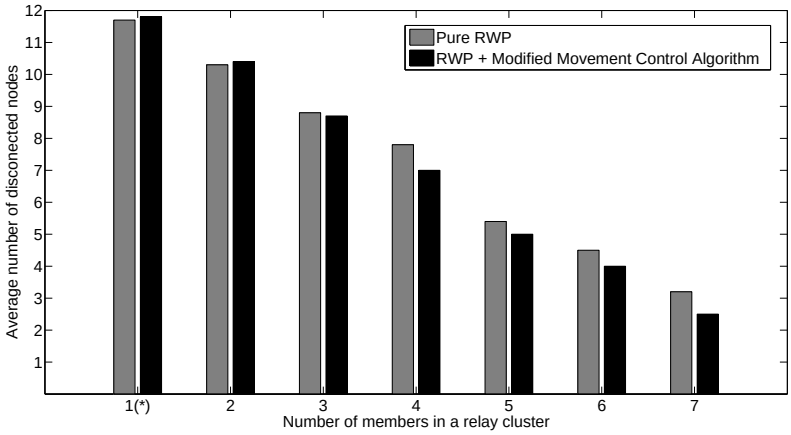

Figure 3.35: Average number of nodes disconnected from sink in relation to the increasing numbers of MIMO cooperating nodes and movement pattern

Figure 3.35 shows that the usage of the adapted movement control proposed on 3.12 allows benefiting from both the extended range provided by the use of cooperative MIMO and the controlled movement of the UAVs, without the drawbacks related to the movements constraints and deadlocks between UAVs, as it avoids the deadlocks between UAVs and static nodes by weighting the decision to move towards a static node by its maximum communication range.

3.15 Summary

The Cooperative MIMO approach presented was capable of increased energy efficiency over large distances, this approach does not involve intermediary nodes and thus is less susceptible to delay caused by the decode and forward mechanism of most multi-hop transmissions or to delay caused by network congestion. Also when using the Cooperative MIMO approach the transmitting node can guarantee a certain data rate, the same link can be used to confirm the reception of data packages at real time without depending on intermediary nodes. In WSNs nearby nodes will often generate similar or redundant information, with Cooperative MIMO these sensors can use the first step to compress and filter important information in order to avoid redundant traffic on the networks. Cooperative MIMO proved to be a powerful solution for long range communication over WSN obtaining increased energy efficiency and distribution of energy consumption.

A Cooperative MIMO selection scheme is proposed using only standard routing algorithms with minor adaptations. The scheme is tested in simulated networks with nodes a variable number of nodes being disabled randomly. The simulations demonstrate increased energy efficiency, reduced packet delivery delay and allows the same area to be covered by a fully connected network with a much smaller number of nodes.

Simulation results also corroborate that the proposed Cooperative MIMO technique is able to achieve higher efficiency in delivering messages from the static to the mobile nodes. It is possible to obtain a better relation of failed transmissions per successful transmissions while increasing

the amount of data that can be transmitted across the network. This improved efficiency reduces energy usage due to communications, which contribute to increasing the network lifetime. The technique also provides a significant decrease in the mean packet delivery delay across the network.

An approach that employs the Cooperative MIMO techniques and relay networks of mobile nodes to support connectivity in sparse WSN is presented. The results provide evidence of the benefits in combining the two techniques, as they help to address the drawbacks of one another besides achieving better results in terms of network connectivity compared to the isolated usage of each of these techniques, while also providing a reduced communication delay.

Chapter 4

Antenna Array UAV Control

As presented on previous chapters, UAVs and WSNs can be combined to achieve highly efficient networks. In order to keep the network fully autonomous and self contained UAVs must be able to operate without relying on a human pilot, thus they must be able to fully locate themselves and make decisions based on current altitude and attitude. The altimeter is a crucial piece of equipment used to measure the altitude of the UAV and keep it from hitting the ground. Regular altimeters are barometric equipment that rely on atmospheric pressure to estimate the current altitude, a secondary radio altimeter serves the purpose of aiding in the final approach and landing. Radio altimeters function similar to a standard radar system, but instead of measuring the round trip time (RTT), which is the time it takes for a signal to be captured back at the receiver after emission, they rely on the phase difference between the transmitted signal and the received replica to estimate the altitude. Barometers offer the disadvantage of being unable to tell if there is an obstacle close to the airplane, since its estimation depends only on atmospheric pressure, radio altimeters can detect such obstacles but are unable to map the surface unless equipped with mechanical rotating antennas. In this section an antenna array based radio altimeter that is capable of mapping the ground without relying on mechanical components is presented.

In order to fully automate the control of UAVs employed in WSNs, it is of extreme importance to be able to estimate the attitude (pitch, yaw and row) of the UAV, as shown in Figure 4.1. Attitude

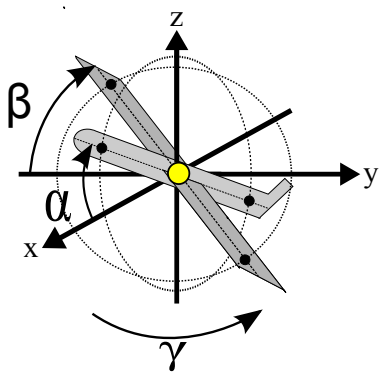

Figure 4.1: Definitions of pitch α, yaw β and roll γ

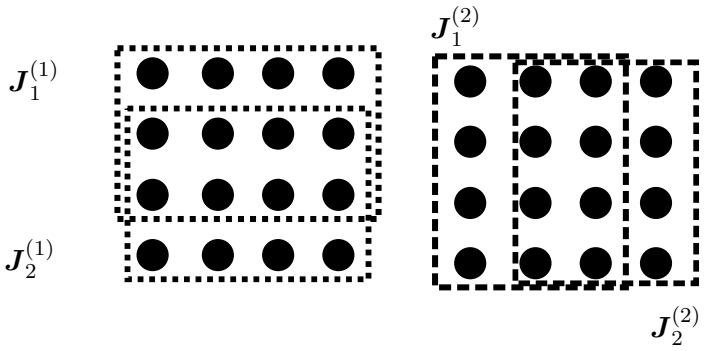

Figure 4.2: Graphical representation of selection matrices

estimation can be performed by using Inertial Measurement Units (IMUs) such as accelerometers and gyroscopes. These units, however, suffer from imprecision caused by measurement and drift errors [29], [30]. Position estimation is usually done with the use of GPS, the satellite information can also be used to provide estimation for the attitude as presented on [31], [32], however, such solutions require additional hardware and require a external element to operate, going against the principle of self containment present of WSNs. Taking advantage of the fact that antenna arrays are currently being implemented into UAVs to enhance communication we can use the available structure to perform the pose estimation. Thus no additional hardware is necessary at the UAV. In [29] an antenna array based attitude estimator has been first proposed. As a drawback of [29] , the prior knowledge of the yaw is required and moreover the proposed solution is severely degraded in scenarios with multipath components. Although, in [33], the constraint of yaw knowledge is relaxed and the solution is extended for multipath scenarios, the numerical precision of the solution has a lower bound even for noiseless scenarios. In this section, a solution assuming that both transmit and receive side are equipped with antenna arrays. In such scenarios is proposed. It is possible not only to increase the accuracy of the attitude estimation, but also to estimate the position of the UAV in space without the use of a GPS system.

4.1 ESPRIT

ESPRIT is a DOA estimation scheme originally proposed in [34] for one dimensional arrays. Extensions exist for multidimensional data for the matrix case [35] and for the tensor case [36]. ESPRIT relies on the Shift Invariance principle, which means that an array can be divided into two subarrays that differ only by an offset. This offset, that can be represented as a phase delay, maps directly to the direction of arrival of a signal.

Figure 4.2 presents the 1-D selection matrices $\boldsymbol{J}_i^{(r)} \in \mathbb{R}^{M_r^{(sel)} \times M_r}$, $i = 1, 2$, these matrices are used to select different sets of $M_r^{(sel)}$ out of M_r elements in order to apply the shift invariance equations.

$$\begin{aligned}\boldsymbol{J}_1^{(r)} &= [\boldsymbol{I}_{M_r^{(sel)}} \mathbf{0}_{M_r^{(sel)} \times 1}], \\ \boldsymbol{J}_2^{(r)} &= [\mathbf{0}_{M_r^{(sel)} \times 1} \boldsymbol{I}_{M_r^{(sel)}}].\end{aligned} \tag{4.1}$$

Using the 1-D selection matrices the R-D selection matrices can be constructed as

$$\begin{aligned}\tilde{\boldsymbol{J}}_1^{(r)} &= \boldsymbol{I}_{\prod_{p=1}^{r-1} M_p} \otimes \boldsymbol{J}_1^{(r)} \otimes \boldsymbol{I}_{\prod_{p=r+1}^{R} M_p}, \\ \tilde{\boldsymbol{J}}_2^{(r)} &= \boldsymbol{I}_{\prod_{p=1}^{r-1} M_p} \otimes \boldsymbol{J}_2^{(r)} \otimes \boldsymbol{I}_{\prod_{p=r+1}^{R} M_p}.\end{aligned} \tag{4.2}$$

A set of shift invariance equations can be constructed for the matrix representation as

$$\begin{aligned}\tilde{\boldsymbol{J}}_1^{(1)} \cdot \boldsymbol{A} \cdot \boldsymbol{\Phi}^{(1)} &= \tilde{\boldsymbol{J}}_2^{(1)} \cdot \boldsymbol{A}, \\ \tilde{\boldsymbol{J}}_1^{(2)} \cdot \boldsymbol{A} \cdot \boldsymbol{\Phi}^{(2)} &= \tilde{\boldsymbol{J}}_2^{(2)} \cdot \boldsymbol{A}, \\ &\vdots \\ \tilde{\boldsymbol{J}}_1^{(R)} \cdot \boldsymbol{A} \cdot \boldsymbol{\Phi}^{(R)} &= \tilde{\boldsymbol{J}}_2^{(R)} \cdot \boldsymbol{A},\end{aligned} \tag{4.3}$$

here the matrices $\boldsymbol{\Phi}^{(r)}$ are given by

$$\boldsymbol{\Phi}^{(r)} = \mathrm{diag}\{[e^{j\mu_1^{(r)}}, e^{j\mu_2^{(r)}}, \ldots, e^{j\mu_d^{(r)}}]\}. \tag{4.4}$$

The matrix $\boldsymbol{A}$ is not known, however, in the absence of noise, the d columns of $\boldsymbol{A}$ and the d columns of the signal signal subspace $\boldsymbol{E}_S$ span the same subspace, and are related by a non singular transform matrix $\boldsymbol{T} \in \mathbb{C}^{d \times d}$

$$\boldsymbol{A} = \boldsymbol{E}_S \cdot \boldsymbol{T}, \tag{4.5}$$

Thus,(4.3) can be rewritten as

$$\begin{aligned}\tilde{\boldsymbol{J}}_1^{(1)} \cdot \boldsymbol{E}_S \cdot \boldsymbol{\Psi}^{(1)} &\approx \tilde{\boldsymbol{J}}_2^{(1)} \cdot \boldsymbol{E}_S, \\ \tilde{\boldsymbol{J}}_1^{(2)} \cdot \boldsymbol{E}_S \cdot \boldsymbol{\Psi}^{(2)} &\approx \tilde{\boldsymbol{J}}_2^{(2)} \cdot \boldsymbol{E}_S, \\ &\vdots \\ \tilde{\boldsymbol{J}}_1^{(R)} \cdot \boldsymbol{E}_S \cdot \boldsymbol{\Psi}^{(R)} &\approx \tilde{\boldsymbol{J}}_2^{(R)} \cdot \boldsymbol{E}_S,\end{aligned} \tag{4.6}$$

where $\boldsymbol{\Psi}^{(r)}$ is related to $\boldsymbol{\Phi}^{(r)}$ by

$$\boldsymbol{\Psi}^{(r)} = \boldsymbol{T} \cdot \boldsymbol{\Phi}^{(r)} \cdot \boldsymbol{T}^{-1}. \tag{4.7}$$

This transformation does not change the eigenvalues present, hence, the eigenvalues of $\boldsymbol{\Psi}^{(r)}$ are equal to $e^{j\mu_1^{(r)}}, e^{j\mu_2^{(r)}}, \ldots, e^{j\mu_d^{(r)}}$. Solving the equation system presented in (4.6) the spatial frequencies of the d signals can be estimated, and thus yields an estimation of the DOAs.

Similarly, a set of shift invariance equations can be written in the tensor representation

$$\begin{aligned}\boldsymbol{\mathcal{A}} \times_1 \boldsymbol{J}_1^{(1)} \times_{R+1} \boldsymbol{\Phi}^{(1)} &= \boldsymbol{\mathcal{A}} \times_1 \boldsymbol{J}_2^{(1)}, \\ \boldsymbol{\mathcal{A}} \times_2 \boldsymbol{J}_1^{(2)} \times_{R+1} \boldsymbol{\Phi}^{(2)} &= \boldsymbol{\mathcal{A}} \times_2 \boldsymbol{J}_2^{(2)}, \\ &\vdots \\ \boldsymbol{\mathcal{A}} \times_R \boldsymbol{J}_1^{(R)} \times_{R+1} \boldsymbol{\Phi}^{(R)} &= \boldsymbol{\mathcal{A}} \times_R \boldsymbol{J}_2^{(R)}.\end{aligned} \tag{4.8}$$

as with the matrix case the $(R+1)$-unfolding of tensor $\boldsymbol{\mathcal{A}}$ and $\boldsymbol{\mathcal{E}}_S$ possess on its rows the basis for the same subspace. Thus there exists a non singular matrix $\boldsymbol{T} \in \mathbb{C}^{d\times d}$ that relates $\boldsymbol{\mathcal{A}}$ and $\boldsymbol{\mathcal{E}}_S$ by

$$\boldsymbol{\mathcal{A}} = \boldsymbol{\mathcal{E}}_S \times_{R+1} \boldsymbol{T}. \tag{4.9}$$

In the presence of noise this relationship is only approximate. The unknown tensor $\boldsymbol{\mathcal{A}}$ can be substituted to yield

$$\begin{aligned}
\boldsymbol{\mathcal{E}}_S \times_1 \boldsymbol{J}_1^{(1)} \times_{R+1} \boldsymbol{\Psi}^{(1)} &\approx \boldsymbol{\mathcal{E}}_S \times_1 \boldsymbol{J}_2^{(1)}, \\
\boldsymbol{\mathcal{E}}_S \times_2 \boldsymbol{J}_1^{(2)} \times_{R+1} \boldsymbol{\Psi}^{(2)} &\approx \boldsymbol{\mathcal{E}}_S \times_2 \boldsymbol{J}_2^{(2)}, \\
&\vdots \\
\boldsymbol{\mathcal{E}}_S \times_R \boldsymbol{J}_1^{(R)} \times_{R+1} \boldsymbol{\Psi}^{(R)} &\approx \boldsymbol{\mathcal{E}}_S \times_R \boldsymbol{J}_2^{(R)}.
\end{aligned} \tag{4.10}$$

Solving the set of tensor equations 4.10 by means of multilinear least squares yields estimates for $\boldsymbol{\Psi}^{(r)}$.

Note that the estimates of the DOAs are not automatically paired over all dimensions, this can be done either by a Maximum Likelihood approach or via the joint diagonalization method proposed in [37]. Also, increased accuracy can be obtained by employing forward-backward averaging as proposed in [38].

4.2 Principles of Radio Altimeters

Radio altimeters usually employ saw tooth wave forms as a modulating signal in order to avoid the distortion caused by the Doppler shift effect [39], this is specially important since aircrafts usually move at high speeds. The frequency usually ranges from 50 Hz to 300 Hz, frequencies bellow this will suffer from higher distortion from Doppler shift while frequencies above will result in a higher bandwidth at the output, this in turn increases the bandwidth of the noise, resulting in a lower SNR. Radio altimeters usually operate at the 4.3 GHz band, with frequency deviations in the order of $\pm$100MHz. Output power ranges anywhere from 10 dBm to 27 dBm. Antennas are designed to offer around 10 dBi directivity in order to cover a wide ground area.

Figure 4.3 presents a simplified block diagram of a conventional radio altimeter. The transmitted signal is generated, as usual FM modulations, by using a voltage-controlled oscillator (VCO). The output of the VCO is then transmitted through the transmitting antennas and also used as the reference local oscillator (LO) at the mixer used for signal demodulation. The scattered signal, received at the receiving antenna, is mixed with the LO signal, creating an intermediate frequency (IF) signal and a higher frequency filtered by the low pass filter. The IF signal is then used to calculate the altitude of the aircraft.

The VCO is a device usually employed for FM modulation and demodulation, the signal generate at the output of the VCO has a frequency controlled by the amplitude of the signal at its input. The frequency at the output of the VCO can be written as

$$f_{\text{VCO}}(t) = f_0 + K \cdot v_{in}(t), \tag{4.11}$$

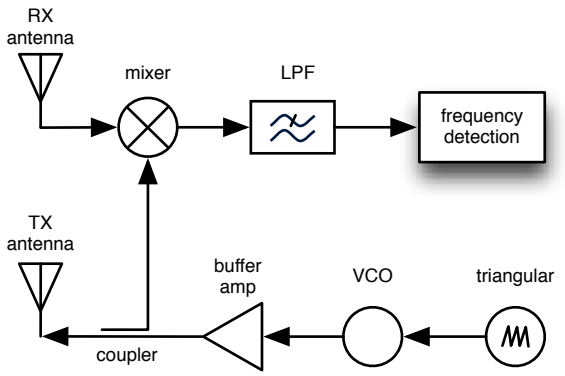

Figure 4.3: Simplified block diagram of a radio altimeter

where f_0 is the center frequency of the VCO, K is known as the gain of the VCO and $v_{in}(t)$ is the amplitude at the input of the VCO at time instant t. Since the instantaneous frequency of a given FM signal is defined as

$$f_i(t) = f_c + \Delta f \cdot m(t), \tag{4.12}$$

where f_c is the carrier frequency, $m(t)$ is the modulating signal and Δf is known as the frequency deviation or the maximum frequency shift of the FM signal, assuming $m(t)$ is limited at ± 1. Its easy to notice the direct relation that exists between the output of the VCO and FM modulation, thus a VCO is commonly used to produce FM modulated signals.

In the case of radio altimeters, the modulated signal is a triangular saw tooth shaped wave, as previously stated. The signal at the input of the VCO can be written as

$$v_{in}(t) = A_0 \cdot m_{\text{saw tooth}}(2\pi f_m t), \tag{4.13}$$

where A_0 is the peak amplitude of the saw tooth wave and f_m is the frequency of the saw tooth wave. A period of $m_{\text{saw tooth}}$ is defined as

$$m_{\text{saw tooth}}(t) = \begin{cases} \frac{4t}{T} - 1 & \text{for } 0 < t \leq \frac{T}{2} \\ \frac{-4t}{T} + 3 & \text{for } \frac{T}{2} < t \end{cases}, \tag{4.14}$$

where $T = \frac{1}{f_m}$. Thus, assuming A_0 is chosen so to limit the amplitude of the signal to ± 1, the output frequency of the VCO using a saw tooth wave as a modulating wave is given by

$$f_i(t) = f_c + \Delta f \cdot m_{\text{saw tooth}}(2\pi f_m t). \tag{4.15}$$

The phase term of a FM signal is given by

$$\xi(t) = 2\pi \int_0^t f_i(t')dt' = 2\pi[f_c t + \Delta f \int_0^t m_{\text{saw tooth}}(t')dt], \tag{4.16}$$

yielding the signal

$$t_x(t) = \cos(\xi(t)) \tag{4.17}$$

at the output of the VCO.

The time delay between transmission of the signal by the UAV and its detection after reflection on the ground is given by

$$\tau(h) = \frac{2 \cdot h}{c}, \tag{4.18}$$

where h is the altitude of the UAV in relation to the point of reflection and c is the speed of light. The amplitude of the signal suffers an attenuation given by α. The received signal can be written as

$$r_x(t) = \alpha \cdot t_x(t - \tau(h)).$$

After being amplified by a factor β the received signal is mixed with an internal copy of the transmitted signal that is provided by the output of the VCO. This is equivalent to performing a FM demodulation on the received signal, but since the internal copy of the signal is out of phase with the received signal due to the time delay suffered, the output of the mixer is given by

$$r_{x\,\mathrm{demod}}(t) = \frac{\beta\alpha}{2}[\cos(\xi(t) - \xi(t - \tau(h))) + \cos(\xi(t) + \xi(t - \tau(h)))]. \tag{4.19}$$

The high frequency term $\cos(\xi(t) + \xi(t - \tau))$ is filtered by the low pass filter. The frequency of the filtered signal is directly related to the time delay of the received signal and can be written as

$$\begin{aligned} f_{r_{x\,\mathrm{demod}}}(\tau(h)) &= f_i(t) - f_i(t - \tau(h)) \\ &= \Delta f \cdot [f_c + \frac{4t}{T} - 1 - f_c - \frac{4(t - \tau(h))}{T} + 1] \\ &= \Delta f \cdot \frac{4\tau(h)}{T} \\ &= 4 \cdot \Delta f \cdot f_m \cdot \tau(h). \end{aligned} \tag{4.20}$$

Replacing (4.18) in (4.20) yields

$$f(h) = \frac{8 \cdot \Delta f \cdot f_m \cdot h}{c}, \tag{4.21}$$

thus the altitude can be estimated by the frequency of the signal at the output of the demodulator.

Altitude estimation can be done by applying the Fourier transform to the signal at the output of the demodulator and looking for the frequency term with peak amplitude [40].

4.3 Antenna Array Radio Altimeter

Traditional radio altimeters are unable to detect multiple obstacles and their location in relation to the UAV. The signal which reflects on the point of lowest altitude is likely to be detected and hide the signals arriving from higher altitudes as shown in Figure 4.5

A signal-to-interference ratio can be defined as the

$$SIR = 10\log_{10}(\frac{P_{LOS}}{P_{NLOS}}), \tag{4.22}$$

where P_{LOS} is the power of the line of sight component and P_{NLOS} is the power of the non line of sight component. If $P_{NLOS} > P_{LOS}$ the NLOS component will be detected. Figure 4.6 presents

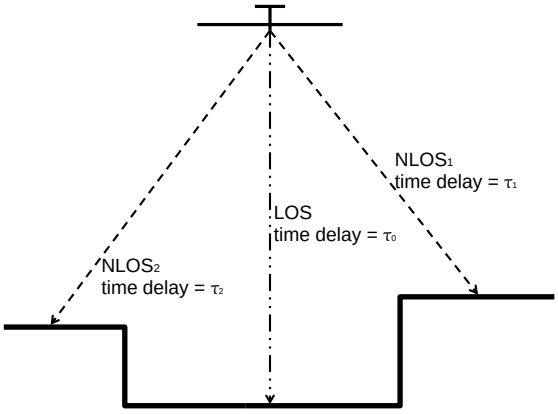

Figure 4.4: Scenario with multiple points of reflection at different altitudes

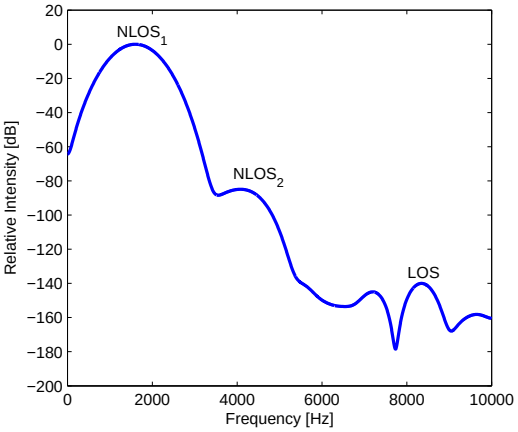

Figure 4.5: Fourier spectrum of the signal received from scenario depicted in Figure 4.4

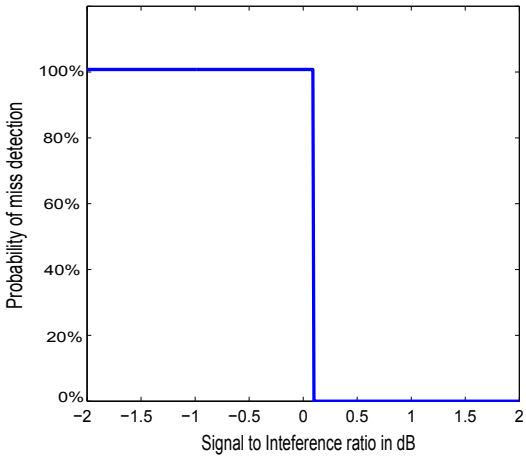

Figure 4.6: Probability of miss detection versus SIR in dB

the probability of detecting the NLOS component in relation to the SIR, once the power of the NLOS component becomes greater then the power of the LOS component the altitude of the NLOS component is detect as the true altitude.

In order to avoid collisions, detecting the strongest signal is a safe practice. However, it is possible to effectively map the ground bellow the UAV and allow it to make decisions based on its entire topology without relying on a mechanical rotating antenna. Rotating antennas rely on electric motors, resulting in a heavy equipment that might make their application impossible, since UAVs usually work with very limited weight constrains. By applying the DOA estimation technique presented on Section 4.1 a software based beam forming can be employed in order not only to detect the altitude of the UAV in relation to obstacles on the ground but also its position.

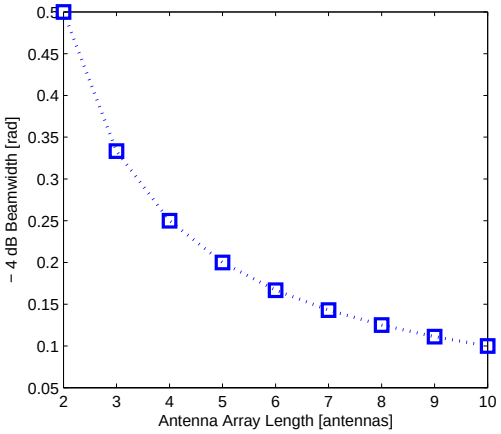

Figure 4.7: -4 dB beam-width vs. number of antennas in the antenna array

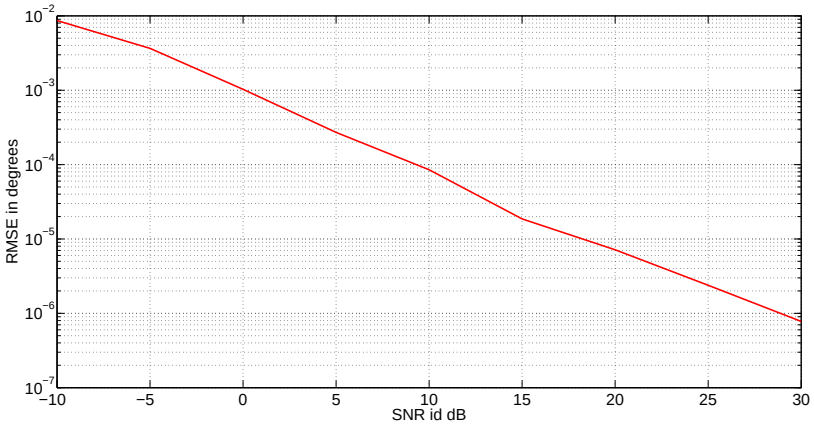

Figure 4.8: RMSE of DOA estimation is degrees

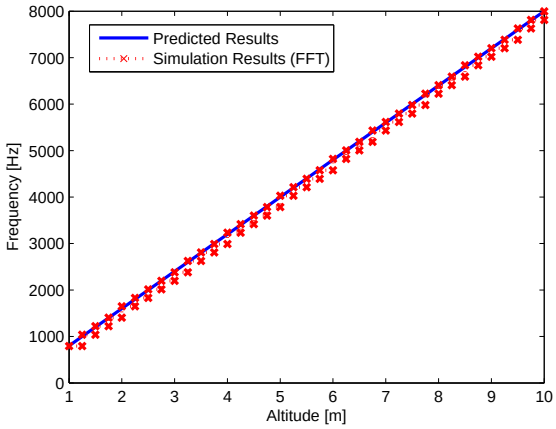

Figure 4.9: Comparison between predicted and simulational results of frequency versus altitude after DOA filtering

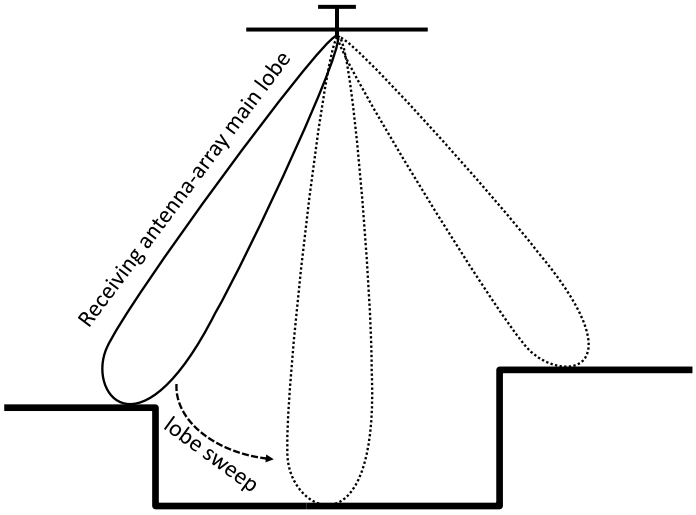

Figure 4.10: Digital lobe sweep using antenna arrays

The resolution of the DOA estimation and thus of the mapping depends on the number of antennas present at the antenna array, more antennas result in a narrower lobe, thus increasing the mapping resolution. Figure 4.7 shows how the resolution increases with the size of the antenna array.

Figure 4.8 presents the RMSE of the DOA estimation versus the SNR for a URA of size 8×8 with two signals present. Even for negative SNR scenarios the estimation yields results with a precision in the order of 10^{-2} degrees. This results in practically no distortion being present on the filtered signal, which in turn yields a very precise altitude estimation. Figure 4.9 presents the results for the altitude estimation after filtering. Due to the discrete nature of the FFT the simulation results present a step-like distribution. It is easy to notice that due to high precision of the DOA estimates, the altitude estimation is highly precise.

4.4 Antenna Array Based Positioning System

The MIMO system is composed of URA at the base station and an antenna array at the UAV as shown in Figure 4.11. The URA is the center of the 3-D space formed by x, y and z. The UAV transmits tonal narrow band signals that are captured by the URA at the base station. Signals can be separated by frequency, orthogonal pulse shaping, or by being transmitted at different time slots.

4.4.1 DOA Estimation

The first step necessary in determining the position of the UAV is to estimate the DOAs, azimuth θ and elevation ϕ, of the signals transmitted by the different UAV antennas. This can be done by employing the ESPRIT algorithm presented on Section 4.1.

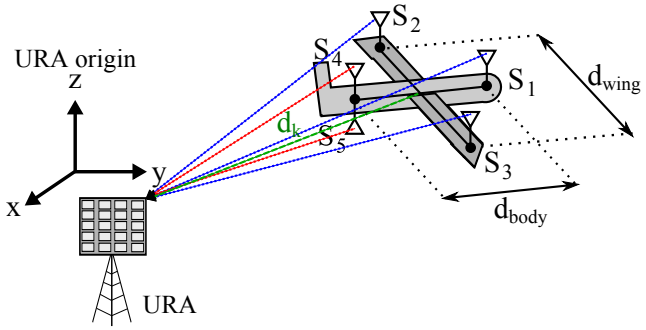

Figure 4.11: System model composed of a URA at the base station and an antenna array at the UAV

4.4.2 Direction Vector Generation

Once the DOAs have been estimated the next step in the process is to generate a direction vector for the line representing the signals. The center of the URA is considered to be the origin of our coordinate system and shall be denoted as O. It is assumed the URA can be made small enough in order for incoming wave front to be represented as lines. Antennas are considered as points in the space and are contained within the line representing the signal they emit. Since the URA is the origin of the coordinate system, all signal lines pass through the origin, an thus a equation representing the coordinates x_{P_i}, y_{P_i} and z_{P_i} of any point P_i contained within the line representing the i-th signal can be written as

$$\begin{aligned} x_{P_i} &= \|m_{P_i}\| \cdot \sin(\phi_i)\cos(\theta_i), \\ y_{P_i} &= \|m_{P_i}\| \cdot \sin(\phi_i)\sin(\theta_i), \\ z_{P_i} &= \|m_{P_i}\| \cdot \cos(\phi_i), \end{aligned} \tag{4.23}$$

where θ_i and ϕ_i are the azimuth and elevation of the i-th signal respectively and $\|m_{P_i}\| \in \mathbb{R}$ is the magnitude of the vector $\vec{OP_i}$.

4.4.3 Position Estimation

After obtaining the direction vector for all signals, an estimate the positions of the antennas on the coordinate system can be obtained by solving a system of equations based on the distance between each pair of antennas. The euclidean distance between two points $A \in \mathbb{R}^3$ and $B \in \mathbb{R}^3$ is given by

$$m_{\vec{AB}} = \sqrt{(x_A - x_B)^2 + (y_A - y_B)^2 + (z_A - z_B)^2}, \tag{4.24}$$

To find the estimate of the point where antennas i and j are located x_A, x_B, y_A, y_B, z_A and z_B can be replaced by x_{P_i}, x_{P_j}, y_{P_i}, y_{P_j}, z_{P_i} and z_{P_j} respectively. Since the distances between each pair of antenna and the DOAs of each signal are known, $\|m_{P_i}\|$ and $\left\|m_{P_j}\right\|$ can be obtained, yielding an estimation for the positions of antenna i and j relation to the center of the URA. Note that we have $n(n-1)/2$ available equations to choose from, where n is the number of antennas present at the UAV.

4.4.4 Attitude Estimation

Once the positions of each antenna present at the UAV have been estimated an estimation of the attitude can be obtained. The TRIAD [41, 42] algorithm proposed by Black allowed the development of early satellite navigation systems and still represents the state of practice for space and aircraft instrument based attitude estimation. It involves only two linear independent reference vectors and their respective measured directions.

By defining two linearly independent reference vectors

$$\begin{aligned} \vec{R}_1 &= [x_{\vec{R}_1}, y_{\vec{R}_1}, z_{\vec{R}_1}]^T, \\ \vec{R}_2 &= [x_{\vec{R}_2}, y_{\vec{R}_2}, z_{\vec{R}_2}]^T, \end{aligned} \tag{4.25}$$

and their respective measured direction vectors

$$\begin{aligned} \vec{r}_1 &= [x_{\vec{r}_1}, y_{\vec{r}_1}, z_{\vec{r}_1}]^T, \\ \vec{r}_2 &= [x_{\vec{r}_2}, y_{\vec{r}_2}, z_{\vec{r}_2}]^T. \end{aligned} \tag{4.26}$$

The TRIAD algorithm tries to find a certain rotation $\boldsymbol{B}$ matrix that satisfies

$$\vec{r_i} = \boldsymbol{B}\vec{R}i, \tag{4.27}$$

where $\boldsymbol{B}^T\boldsymbol{B} = \boldsymbol{I}$ and $\det(\boldsymbol{B}) = \pm 1$, i.e $\boldsymbol{B}$ is a orthogonal matrix and preserves the magnitude of vectors it operates on. Since $\vec{R}_1$ and $\vec{R}_2$ are linearly independent vectors, a linear independent vector orthogonal to both can by obtained by

$$\vec{R}_3 = \vec{R}_1 \times \vec{R}_2, \tag{4.28}$$

where $\times$ represent the vector cross product operation, the same can be done for $\vec{r}_1$ and $\vec{r}_2$

$$\vec{r}_3 = \vec{r_1} \times \vec{r}_2. \tag{4.29}$$

Since a rotation applied to $\vec{R}_1$ and $\vec{R}_2$ would also rotate $\vec{R}_3$, a linear system can be written as

$$[\vec{r}_1, \vec{r}_2, \vec{r}_3] = \boldsymbol{B}[\vec{R}_1, \vec{R}_2, \vec{R}_3]. \tag{4.30}$$

In the noise free case the present linear system holds exact and will yield a orthogonal matrix $\boldsymbol{B}$. However, in the presence of noise, the result might be a non orthogonal matrix. To address this problem the TRIAD algorithm operates replaces $\vec{R}_1$, $\vec{R}_2$ and $\vec{R}_3$ by

$$\begin{aligned} \vec{S}_1 &= \frac{\vec{R}_1}{\left\|\vec{R}_1\right\|}, \\ \vec{S}_2 &= \frac{\vec{R}_1 \times \vec{R}_2}{\left\|\vec{R}_1 \times \vec{R}_2\right\|}, \\ \vec{S}_3 &= \frac{\vec{S}_1 \times \vec{S}_2}{\left\|\vec{S}_1 \times \vec{S}_2\right\|}. \end{aligned} \tag{4.31}$$

respectively. And $\vec{r}_1$, $\vec{r}_2$ and $\vec{r}_3$ by

$$\begin{aligned}\vec{s}_1 &= \frac{\vec{r}_1}{\|\vec{r}_1\|},\\ \vec{s}_2 &= \frac{\vec{r}_1 \times \vec{r}_2}{\|\vec{r}_1 \times \vec{r}_2\|},\\ \vec{s}_2 &= \frac{\vec{s}_1 \times \vec{s}_2}{\|\vec{s}_1 \times \vec{s}_2\|}.\end{aligned} \tag{4.32}$$

respectively. Note that by construction the matrices $[\vec{S}_1, \vec{S}_2, \vec{S}_3]$ and $[\vec{s}_1, \vec{s}_2, \vec{s}_3]$ are orthogonal matrices, since their columns are made orthogonal to each other. This avoids the computationally intensive task of calculating the matrix inverse, since $[\vec{S}_1, \vec{S}_2, \vec{S}_3]^{-1} = [\vec{S}_1, \vec{S}_2, \vec{S}_3]^T$. Thus, an estimate of $\boldsymbol{B}$ can be found by

$$\hat{\boldsymbol{B}} = [\vec{s}_1, \vec{s}_2, \vec{s}_3][\vec{S}_1, \vec{S}_2, \vec{S}_3]^T. \tag{4.33}$$

As the rotation matrix is directly dependent on the pitch, yaw and roll an estimation can be extracted from $\hat{\boldsymbol{B}}$. The yaw, pitch and roll rotation matrices are given by

$$\begin{aligned}\boldsymbol{R}(\alpha) &= \begin{bmatrix} \cos(\alpha) & -\sin(\alpha) & 0 \\ \sin(\alpha) & \cos(\alpha) & 0 \\ 0 & 0 & 1 \end{bmatrix},\\ \boldsymbol{R}(\beta) &= \begin{bmatrix} \cos(\beta) & 0 & \sin(\beta) \\ 0 & 1 & 0 \\ -\sin(\beta) & 0 & \cos(\beta) \end{bmatrix},\\ \boldsymbol{R}(\gamma) &= \begin{bmatrix} 1 & 0 & 0 \\ 0 & \cos(\gamma) & -\sin(\gamma) \\ 0 & \sin(\gamma) & \cos(\gamma) \end{bmatrix}.\end{aligned} \tag{4.34}$$

If the rotation follows the order of yaw, pitch and roll, then

$$\hat{\boldsymbol{B}} = \boldsymbol{R}(\alpha)\boldsymbol{R}(\beta)\boldsymbol{R}(\gamma) =$$

$$\hat{\boldsymbol{B}} = \begin{bmatrix} \cos(\hat{\alpha})\cos(\hat{\beta}) & \cos(\hat{\alpha})\sin(\hat{\beta})\sin(\hat{\gamma}) - \sin(\hat{\alpha})\cos(\hat{\gamma}) & \cos(\hat{\alpha})\sin(\hat{\beta})\cos(\hat{\gamma}) + \sin(\hat{\alpha})\sin(\hat{\gamma}) \\ \sin(\hat{\alpha})\cos(\hat{\beta}) & \sin(\hat{\alpha})\sin(\hat{\beta})\sin(\hat{\gamma}) - \cos(\hat{\alpha})\cos(\hat{\gamma}) & \sin(\hat{\alpha})\sin(\hat{\beta})\cos(\hat{\gamma}) + \cos(\hat{\alpha})\sin(\hat{\gamma}) \\ -\sin(\hat{\beta}) & \cos(\hat{\beta})\sin(\hat{\gamma}) & \cos(\hat{\beta})\cos(\hat{\gamma}) \end{bmatrix}, \tag{4.35}$$

where $\hat{\alpha}$, $\hat{\beta}$ and $\hat{\gamma}$ are estimates of the yaw pitch and roll respectively. Note that changing the order of rotation will change the structure of $\hat{\boldsymbol{B}}$.

The TRIAD algorithm allows an estimate of the UAV attitude to be obtained by obtaining only two linearly independent position vectors, such as a wing and the nose position vectors. Other methods for estimating the attitude exist, such as the QUEST [43, 44, 45] and SVD based methods such as [46]. These methods are capable of taking into account a broad set of measurements and reference vectors resulting a more accurate estimation. However, they are more computationally intensive then the TRIAD algorithm and usually much slower.

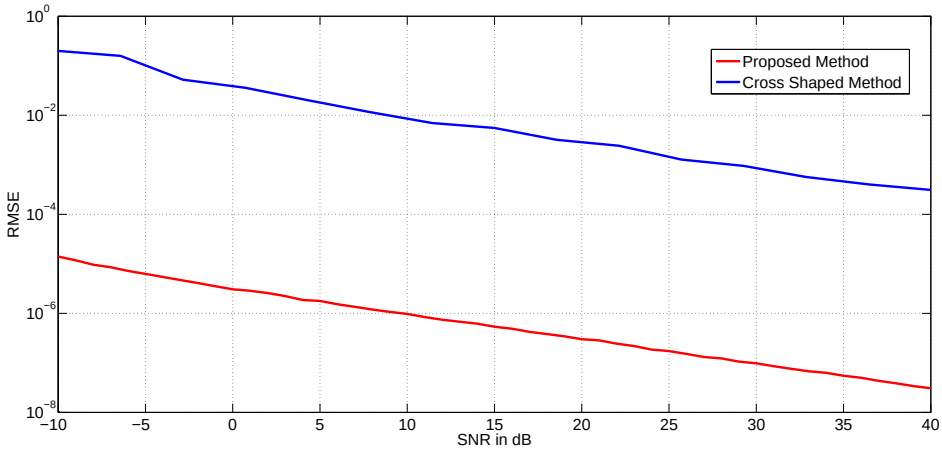

Figure 4.12: RMSE of estimates of the pitch, yaw and roll vs the signal to noise ratio (SNR)

4.5 Results for Attitude Estimation

Figure 4.12 presents a comparison between the proposed method and the one proposed on [33]. In the simulation the UAV is placed at 1000 m from the base station and the URA is of size 10 by 10. Note that the high accuracy of the ESPRIT already presented in Figure 4.8 yields a very accurate estimation of the UAV attitude.

4.6 Summary

This section presented a antenna array based altimeter and a antenna array based positioning system.

The proposed altimeter solution allows to estimate not only the altitude, but also the inclination of the ground as well as possible obstacles and topology, resulting in a safer automated flight and integration with WSNs, allowing UAVs to automate altitude based decision making. This allows UAVs to employed in the context of independent and self contained WSNs.

The proposed position estimation method is capable of estimating the precise position and attitude of an UAV in space without requiring prior knowledge of pitch, yaw or roll. Also, no GPS is necessary and the distance from UAV to base station can easily be obtained once the position has been estimated. Simulations show that the technique is robust and capable of performing in a robust manner even at low SNR scenarios. With attitude and position estimation the task of UAV controlling can be fully automated, allowing the insertion of UAV in independent and self contained WSNs. The attitude and positioning estimation can be used in conjunction with the scheme proposed on Chapter 3 to keep networks connected even when nodes start to fail.

Chapter 5

Conclusion

In this work the problem of limited energy budget in WSNs and their interaction with mobile nodes is addressed. A set of tools taking advantage of the cooperative nature of WSNs is developed and presented, capable of reducing energy cost and enhancing communication between static and mobile nodes. Taking advantage of the set of antennas present in the mobile nodes, a set of techniques is developed in order to achieve increased precision in the control of this nodes without relying on external elements.

The first part presents a brief introduction to tensor algebra, a representation capable of properly storing the information of R-dimensional data. The r-mode product, unfolding and the HOSVD, an extension of the matrix SVD, are presented. These tools allow the manipulation of tensors very similarly to the matrix form without sacrificing the information related to the structure of the data.

The second part is related to the study of the application of array signal processing the WSNs. First the energy consumption of standard multi-hop and single-hop communications are studied, their point of optimal operation is derived in order to obtain a standard of comparison. The basics of MIMO communication are presented and the BER of multiple MIMO channel equalization techniques is compared with standard SISO communication. The Cooperative MIMO communication scheme for WSNs is presented and its improvements for long range communications are shown by means of simulations. The limitation of the proposed technique for short range communications is also presented and discussed. An automatic selection method for opting between the optimal Cooperative MIMO configuration, in terms of cluster size, for long range and standard techniques for short range is presented. The proposed method acts as an extension of a standard routing algorithm and requires only minor software changes, allowing it to be employed in WSNs currently in operation. The behavior of a network subject to random node failures is studied and the benefits of automatic selection when compared to fixing a Cooperative MIMO cluster size are shown. The relationship between Cooperative MIMO networks and fast moving mobile nodes is studied. The increased data rate or range achievable through Cooperative MIMO is shown to allow efficient communication in hybrid networks, increasing throughput and reducing transmission failures and packet delivery delay. To take advantage of the increased efficiency in hybrid networks an algo-

rithm for controlling the movement of mobile nodes sparse networks is presented. The algorithm is shown to increase network connectivity in WSNs composed of node clusters separated by large distances.

Finally, in the third part the presence of antenna arrays for communication in the mobile nodes is further explored. An improved radio altimeter capable of mapping the entire ground topology is presented and its efficiency is shown by means of simulations. An antenna array based position and attitude estimation system is proposed. The system is shown to be capable of efficient attitude estimation without relying on traditional IMUs or systems external to the WSN such as GPS systems.

REFERENCES

[1] I. Akyildiz, W. Su, Y. Sankarasubramaniam, and E. Cayirci, "Wireless sensor networks: a survey," *Computer Networks*, vol. 38, pp. 393–422, 2002.

[2] Y. Liang and W. Peng, "Minimizing Energy Consumptions in Wireless Sensor Networks via Two-Modal Transmission," *ACM SIGCOMM Computer Communication Review*, vol. 40, pp. 13 – 18, 2010.

[3] S. Cho and A. Chandrakasan, "Energy-efficient protocols for low duty cycle wireless microsensor," in *Proceedings of the 33rd Annual Hawaii International Conference on System Sciences*, 2000.

[4] P. Lettieri and M. B. Srivastava, "Adaptive frame length control for improving wireless link throughput, range and energy efficiency," in *INFOCOM '98. Seventeenth Annual Joint Conference of the IEEE Computer and Communications Societies. Proceedings. IEEE*, 1998.

[5] W. R. Heinzelman, A. Chandrakasan, and H. Balakrishnan, "Energy-efficient communication protocol forwireless microsensor networks," in *Proceedings of the 33rd Hawaii International Conference on System Sciences*, 2000.

[6] D. Ganesan, R. Govindan, S. Shenker, and D. Estrin, "Highly-resilient, energy-efficient multipath routing in wireless sensor networks," *ACM SIGMOBILE Mobile Computing and Communications Review*, vol. 5, no. 4, p. 1125, 2001.

[7] M. Weiser, B. Welch, A. Demers, and S. Shenker, "Scheduling for reduced cpu energy," in *Proceedings of 1st USENIX Symposium on Operating System Design and Implementation*, November 1994, pp. 13–23.

[8] E. Shih, B. H. Calhoun, S. Cho, and A. P. Chandrakasan, "Energy-efficient link layer for wireless microsensor networks," in *VLSI, 2001. Proceedings. IEEE Computer Society Workshop on*, 2001.

[9] E. Shih, S. Cho, N. Ickes, R. Min, A. Sinha, and A. C. A. Wang, "Physical layer driven protocol and algorithm design for energy-efficient wireless sensor networks," in *Proceedings of ACM MobiCom01*, 2001.

[10] D. Jea, A. Somasundara, and M. Srivastava, "Multiple controlled mobile elements (data mules) for data collection in sensor networks," in *Distributed Computing in Sensor Systems, First*

IEEE International Conference, DCOSS 2005, Proceedings, Marina del Rey, CA, USA, July 2005.

[11] M. Wax and T. Kailath, "Detection of signals by information by information theoric criteria," *IEEE Transactions on Acoustics Speech and Signal Processing*, vol. 33, pp. 387–392, 1985.

[12] J. P. C. L. da Costa, M. Haardt, F. Romer, and G. Del Galdo, "Enhanced model order estimation using higher-order arrays," *Conference Record of The Forty-First Asilomar Conference on Signals, Systems & Computers*, pp. 412–416, 2007.

[13] L. De Lathauwer, B. De Moor, and J. Vandewalle, "A multilinear singular value decomposition," in *SIAM J. Matrix Anal*, 2000.

[14] E. P. Freitas, J. P. C. L. Costa, A. L. F. Almeida, and M. A. M. Marinho, "Applying mimo techniques to minimize energy consumption for long distances communications in wireless sensor networks," in *NEW2AN/ruSMART 2012*, Springer-Verlag, Ed., 2012, pp. 379–390.

[15] E. P. Freitas, T. Heimfarth, I. F. Netto, C. E. Lino, A. M. F. F. R. Wagner, C. E. Pereira, and T. Larsson, "UAV relay network to support WSN connectivity," in *Proceedings of IEEE International Congress on Ultramodern Telecommunications and Control Systems (ICUMT10)*, 2010.

[16] D. Couto, D. Aguayo, J. Bicket, and R. Morris, "A high-throughput path metric for multi-hop wireless routing," *Wirel. Netw*, vol. 11, pp. 419–435, 2005.

[17] W. Lou, W. Liu, and Y. Zhang, "Performance optimization using multipath routing in mobile ad hoc and wireless sensor networks," *Combinator. Optim. Commun. Netw.*, vol. 2, pp. 117–146, 2006.

[18] A. Woo, T. Tong, and D. Culler, "Taming the underlying challenges of reliable multihop routing in sensor networks," in *Proc. ACM SenSys 2003*, 2003.

[19] C. Chen, J. Ma, and K. Yu, "Designing energy-efficient wireless sensor networks with mobile sinks," in *Sensys06*, 2006.

[20] M. Bhardwaj and A. P. Chandrakasan, "Upper bounds on the lifetime of sensor networks," in *Proceedings of IEEE ICC01*, 2001.

[21] V. Mhatre and C. Rosenberg, "Design guidelines for wireless sensor networks: communication, clustering and aggregation," in *Elsevier Ad Hoc Networks*, 2004.

[22] P. W. Wolniansky, G. J. Foschini, G. D. Golden, and R. A. Valenzuela, "V-BLAST: An architecture for realizing very high data rates over the rich-scattering wireless channel," in *Bell Laboratories, Lucent Technologies, Crawford Hill Laboratory.*

[23] M. Biguesh and A. B. Gershman, "Training-based MIMO channel estimation: A study of estimator tradeoffs and optimal training signals," *IEEE Transactions on Signal Processing*, vol. 54, pp. 884–893, 2006.

[24] R. Trepkowski, "Channel estimation strategies for coded MIMO systems," Master's thesis, Virginia Polytechnic Institute and State University.

[25] A. J. Viterbi, "Error bounds for convolutional codes and an asymptotically optimum decoding algorithm," *IEEE Transactions on Information Theory*, vol. 13, pp. 260–269, 1967.

[26] S. Lanzisera, A. M. Mehta, and K. S. J. Pister, "Reducing average power in wireless sensor networks through data rate adaptation," in *Proc. IEEE International Conference on Communications*, 2009, pp. 480–485.

[27] N.Zhu, W. Du, D. Navarro, F. Mieyeville, and I. O. Connor, "High data rate wireless sensor networks research," Technical Report.

[28] M. Zhao, M. Ma, and Y. Yang, "Mobile data gathering with multiuser MIMO technique in wireless sensor networks," in *Proc. IEEE GLOBECOM 2007*, 2007.

[29] J. P. C. L. da Costa, S. Schwarz, L. F. de A. Gadlha, H. C. Moura, G. A. Borges, and L. A. R. Pinheiro, "Attitude determination for unmanned aerial vehicles via an antenna array," in *Proc. ITG IEEE Workshop on Smart Antennas (WSA12)*, Dresden Germany, March 2012.

[30] G. L. Sitzmann and G. H. Drescher, "Tactical ballistic missiles trajectory state and error covariance propagation," in *IEEE Position Location and Navigation Symposium.* Las Vegas, NV, USA: IEEE, April 1994, pp. 839–844.

[31] J. Jang, S. Lee, and C. Kee, "Performance enhancement of attitude determination system by combining single and multiple antennas," in *Proc. of the 17th International Technical Meeting of the Satellite Division of The Institute of Navigation (ION GNSS 2004)*, Long Beach, CA, USA, 2004, pp. 2066–2073.

[32] C. Cohen, "Attitude determination using GPS," Ph.D. dissertation, Department of Aeronautics & Astronautics, Stanford University, CA, USA, 1992.

[33] K. Liu, J. P. C. L. da Costa, H. C. So, L. F. A. Gadelha, and G. A. Borges, "Improved attitude determination for unmanned aerial vehicles with a cross-shaped antenna array," in *Proc. IASTED International Conference on Signal and Image Processing (SIP 2012)*, Honolulu, Hawaii, USA, August 2012, pp. 60–67.

[34] R. Roy and T. Kailath, "ESPRIT - estimation of signal parameters via rotation invariance techniques," *IEEE Transactions on Acoustics Speech and Signal Processing*, vol. 17, 1989.

[35] M. Haardt, "Efficient one-, two- and multidimensional high-resolution array signal processing," in *3-8265-2220-6.* Aachen, Germany: Shaker Verlag, 1996.

[36] M. Haardt, F. Roemer, and G. Del Galdo, "Higher-Order SVD-Based Subspace Estimation to Improve the Parameter Estimation Accuracy in Multidimensional Harmonic Retrieval Problems," *IEEE Transactions on Signal Processing*, vol. 56, pp. 3198–3213, 2008.

[37] M. Haardt and J. A. Nossek, "Simultaneous Schur Decomposition of Several Nonsymmetric Matrices to Achieve Automatic Pairing in Multidimensional Harmonic Retrieval Problems," *IEEE Transactions on Signal Processing*, vol. 46, pp. 161–169, 1998.

[38] ——, "Unitary ESPRIT: how to obtain increased estimation accuracy with a reduced computational burden," *IEEE Transactions on Signal Processing*, vol. 43, no. 5, May 1995.

[39] M. Skolnik, *Radar Handbook: Second Edition.* McGraw-Hill, 1991.

[40] M. Vidmar, "A landing radio altimeter for small aircraft," in *12th International Power Electronics and Motion Control Conference*, 2006.

[41] H. Black, "Early developments of transit, the navy navigation satellite system," *Journal of Guidance, Control and Dynamics*, vol. 13, pp. 577 – 585, July-Aug 1990.

[42] ——, "A passive system for determining the attitude of a satellite," *AIAA Journal*, vol. 2, pp. 1350 –1351, July 1964.

[43] M. D. Shuster, "Approximate algorithms for fast optimal attitude computation," in *Proceedings, AIAA Guidance and Control Conference*, 1978.

[44] ——, "Maximum likelihood estimation of spacecraft attitude," *The Journal of the Astronautical Sciences*, vol. 108, pp. 2089–2117, 2001.

[45] ——, "Three-axis attitude determination from vector observations," *Journal of Guidance and Control*, vol. 4, pp. 79–88, 1981.

[46] F. L. Markley, "Attitude determination using vector observations and the singular value decomposition," in *AAS/AIAA Astrodynamics Specialist Conference*, 1987.